POLITECNICO
MILANO 1863

SCUOLA DI INGEGNERIA INDUSTRIALE
E DELL'INFORMAZIONE

Numerical Modelling and Techno-Economic Assessment of a Vacuum Swing Adsorption Process for Post-Combustion CO_2 Capture

TESI DI LAUREA MAGISTRALE IN
ENERGY ENGINEERING
INGEGNERIA ENERGETICA

Author: **Nima Razmjoo**

Student ID: 10702398
Advisor: Manuele Gatti
Co-advisor: Maurizio Spinelli
Academic Year: 2021-22

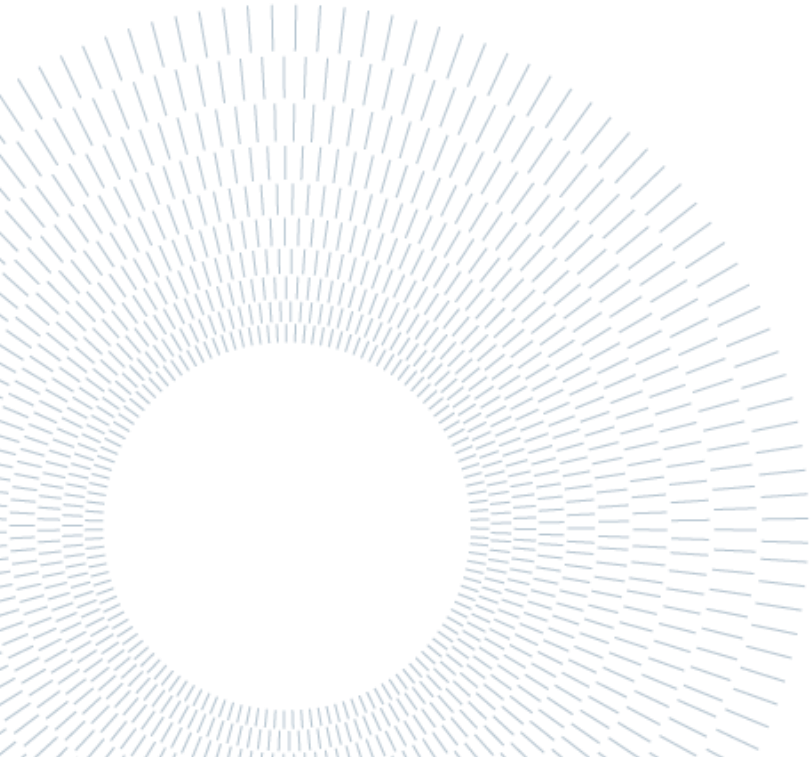

Abstract

Solvent-based systems are currently the benchmark technology for post-combustion CO_2 capture. However, due to the high energy penalty that they impose on the host plant, other alternatives such as the Vacuum-Swing Adsorption (VSA) are raising attention in recent years not only because of the lower energy penalty but also of the sole use of electricity instead of thermal energy which avoids the heat integration complexities to the host plant.

The transient inherent of sorbent-based system's process steps avoids us to use the commercialized process simulation software for process modelling. In this work, we numerically solved the model equations in transient mode using MATLAB aimed at reaching the Cyclic Steady State (CSS) in which the performance of the system is evaluated. The model is then validated using the data from one of the main pioneer literature in this field.

To assess the performance of the system on a large scale, the flue gas data from a 200 MW_{th} WtE plant is used. A cycle scheduling and column sizing methodology is also suggested for supplying a continuous feed to the VSA system while minimizing the footprint of the scaled-up scheme. To reach the final state of 95% purity and 110 bar which is the minimum requirement of a standard CCUS system, the exited stream of the VSA is further treated in a CO_2 Purification Unit (CPU). Three different scenarios are compared in terms of technical and economic performances at different recovery levels. The highest recovery scenario with an overall recovery of 91%, resulted in 397 $\frac{kWh}{t_{CO2\ purified}}$ of electrical energy consumption for the integrated VSA-CPU system. Moreover, the total cost of 108.5 $\frac{€}{t_{CO2\ purified}}$ is calculated based on the electricity price in 2022, which can be decreased by 20% if the price of electricity will set back to its 2020's level.

Key-words: *Vacuum—Swing Adsorption, Numerical Modeling, Post-Combustion CO_2 Capture, Techno-Economic Assessment, CCUS.*

Abstract in italiano

I sistemi a base di solventi sono attualmente la tecnologia di riferimento per la cattura di CO_2 post-combustione. Tuttavia, a causa dell'elevata penalizzazione energetica che impongono all'impianto ospite, negli ultimi anni altre alternative come l'adsorbimento oscillante sottovuoto (VSA) stanno attirando l'attenzione non solo per la minore penalizzazione energetica ma anche per il solo utilizzo di energia elettrica invece dell'energia termica che evita le complessità di integrazione del calore alla pianta ospite.

Il transitorio inerente alle fasi del processo del sistema basato su assorbente ci evita di utilizzare il software di simulazione del processo commercializzato per la modellazione del processo. In questo lavoro, abbiamo risolto numericamente le equazioni del modello in modalità transitoria utilizzando MATLAB finalizzato al raggiungimento del Cyclic Steady State (CSS) in cui vengono valutate le prestazioni del sistema. Il modello viene quindi validato utilizzando i dati di una delle principali pubblicazioni pionieristiche in questo campo.

Per valutare le prestazioni del sistema su larga scala, vengono utilizzati i dati sui fumi di un impianto WtE da 200 MW_{th}. Si suggerisce inoltre una metodologia di pianificazione del ciclo e dimensionamento delle colonne per fornire un'alimentazione continua al sistema VSA riducendo al minimo l'ingombro dello schema in scala. Per raggiungere lo stato finale di purezza del 95% e 110 bar, che è il requisito minimo di un sistema CCUS standard, il flusso in uscita del VSA viene ulteriormente trattato in CO_2 Purification Unit (CPU). Vengono confrontati tre diversi scenari in termini di performance tecniche ed economiche a diversi livelli di ripresa. Lo scenario di recupero più elevato, con un recupero complessivo del 91%, ha comportato un consumo di energia elettrica di $397 \frac{kWh}{t_{CO2\ purificata}}$ per il sistema integrato VSA-CPU. Inoltre, il costo totale di $108.5 \frac{€}{t_{CO2\ purificata}}$ è calcolato sulla base del prezzo dell'elettricità nel 2022, che può essere ridotto del 20% se il prezzo dell'elettricità torna al livello del 2020.

Parole chiave: *Adsorbimento dell'oscillazione del vuoto, Modellazione numerica, Cattura di CO_2 post-combustione, Valutazione Tecno-Economica, CCUS.*

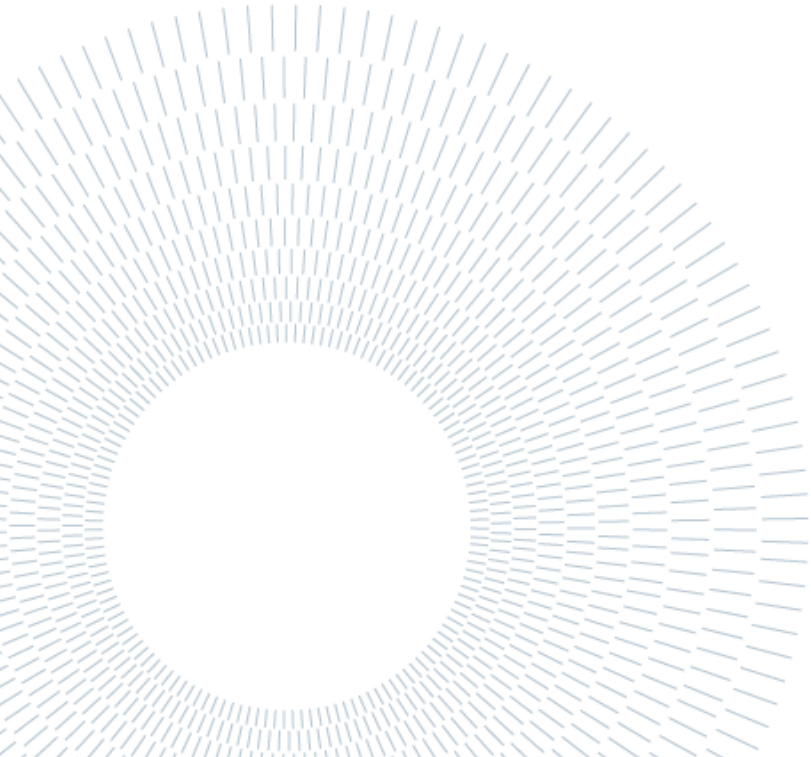

Contents

Introduction

The path towards decarbonizing the energy sector and carbon-intense industries (such as cement, steelmaking, waste-to-energy (WtE), hydrogen production, etc.) not only consists of using renewable sources but, also relies on alternative options such as retrofitting the existing fossil-fired plants with CO_2 capture systems.

One of the main issues that hinder the fast development of the post-combustion CO_2 capture technologies is that such systems are energy and capital-intensive, meaning that they result in a decrease in the net efficiency and cost increase of the host plant. Although solvent-based processes are the benchmark, alternatives such as sorbent-based technologies showed promising performance to cope with the above-mentioned issues.[1]

Sorbent-based gas separation systems are currently implemented in different industries such as syngas purification. To design a continuous system, at least two columns should be in operation simultaneously. While the first one is in operation with adsorbing the target gas component into the sorbent bed, the sorbent bed should be regenerated in the other column to be prepared for the next capture cycle. Two main strategies namely Temperature-Swing Adsorption (TSA) and Pressure-Swing Adsorption (PSA) can be implemented for bed regeneration, utilizing heat and electricity respectively.

Using electricity instead of heat to regenerate the sorbent material could be promising in applications where there are alternative uses of waste heat in the host site. Besides, studies show that in the case of separating CO_2 from post-combustion flue gas, the PSA process performs at a lower energy penalty (considering the transformation of thermal energy into electricity occurs with an efficiency of 30%) compared to either TSA or solvent-based systems.[2,3]

Swing adsorption systems consist of individual process steps which are inherently transient. This is due to the fact that different process steps work in a specified order one after another in a single column, meaning that the column state at the end of a process step, is the initial state of the next process step. Hence, instead of a steady state condition in the column (such as the one solvent-based systems work), we can define Cyclic Steady State (CSS) which shows the steady state condition after a full cycle operation, without any changes in the outputs compared to the previous cycle.

Commercial process modeling software such as Aspen Adsorption is currently under development for such transient processes. Another alternative is to numerically solve the model equations (mass, momentum, and energy balance) in the unsteady condition, which gives us a set of Partial Differential and Algebraic Equations (PDAEs) which should be solved simultaneously. Software such as gPROMS and MATLAB is used to numerically solve these sets of PDAEs.

In this work, we aimed at developing a numerical model using MATLAB for a one-stage 4-step Vacuum-Swing Adsorption (VSA) process in which adsorption occurs at atmospheric pressure while bed regeneration occurs at vacuum pressure levels. The model is then validated against the data from one of the main research references on this topic[4]. Finally, the model is implemented in a case study for the techno-economic evaluation of the system on a large scale.

Although the developed model is applicable in all the post-combustion CO_2 capture, without losing its generality, we considered a large-scale 200 MW_{th} WtE plant as our case study in which the VSA can be applied. The WtE plant is chosen because not only the low energy penalty CO_2 capture is essential in WtE plants as they recover energy at a high cost, but also the sole electricity consumption of VSA which decreases the complexity of heat integration strategies that should be added to the host plant.

Retrofitting the large-scale plants with VSA for CO_2 capture requires further considerations in terms of continuous feed and footprint. As all the swing adsorption systems are batch processes in which the feed needed to be disrupted for sorbent regeneration in the column, to maintain continuous feed into our system several columns should operate simultaneously. The choice of the number of columns requires a complete optimization scheme, taking into account all the operational variables such as pressure levels and step timing, with the objective of maximizing recovery and purity levels.

The methodology that we have followed for the large-scale case study, is based on the objective of reaching the lowest possible footprint while maintaining the continuous feed. This is based on the fact that a large footprint is reported as one of the main issues that currently avoid the development of VSA CO_2 capture to higher TRLs.[3,5] Besides, instead of the full optimization scheme that is beyond the scope of this work, we have performed a sort of parametric analysis which resulted in three scenarios that were further technically and economically evaluated and compared.

In Figure 0.1 the sequence of works and objectives that we have followed in this work is represented.

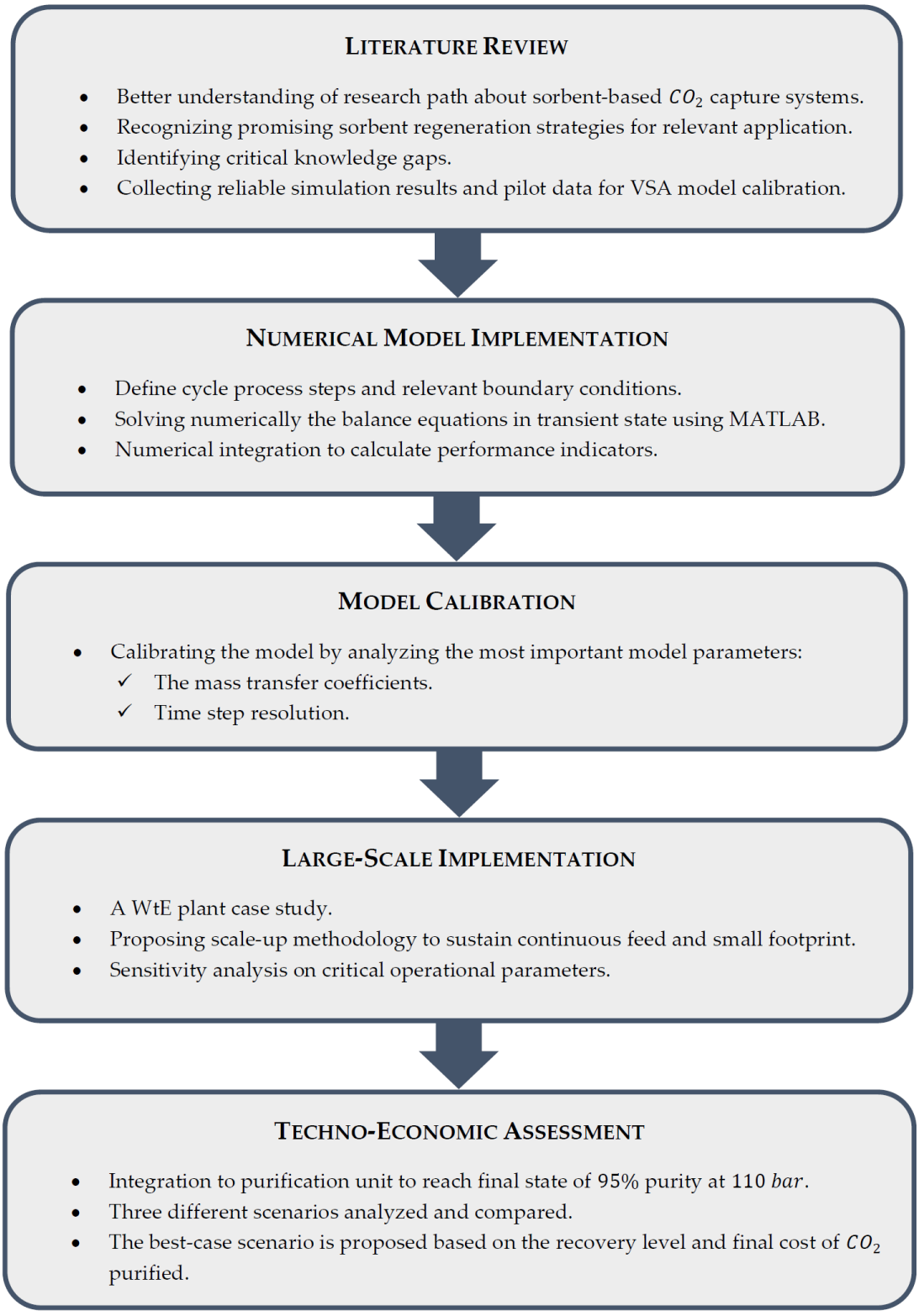

Figure 0.1: General flowchart of the project.

1 Adsorption-based Post-Combustion CO_2 Capture

Research and development about post-combustion CO_2 capture using solid sorbent, aimed at both the development of proper sorbent materials as well as the process configuration itself.[1] In this chapter, sorbent characteristics for this application are discussed by analyzing the relevant literature. Besides, the processes (including both reactor configurations and regeneration strategies) that are currently under development are another subject of the literature review that we performed and reported in this chapter.

1.1. Sorbent materials

The selection of sorbent material is a critical issue in case of post-combustion CO_2 capture. The proper sorbent material should be able to adsorb a relatively high amount of CO_2 in low partial pressure which is the case in the post-combustion flue gas. This is known as the saturation capacity of a sorbent concerning the target adsorbate (CO_2 here). Hence, the proper sorbent should represent high saturation capacity in low CO_2 partial pressures. As the adsorption occurs at relatively high pressure, developing proper material to adsorb CO_2 at such low pressure is quite challenging.

Researchers initially used Activated Carbon data and characteristics in adsorption-based CO_2 capture process modeling.[6] Gradually, the choice of materials changed into Zeolite 13X, as this commercialized sorbent showed proper saturation capacity making it suitable for CO_2 capture from post-combustion flue gas at low partial pressures (Figure 1.1). Hefti et al., measured the pure component isotherms of two commercial Zeolites (ZSM-5 and 13X) which is a good reference in case of process modeling using these materials as sorbents.[7] As we can see, the saturation capacity is relatively high for low partial pressures compared to the two Metal-Organic Frameworks (MOFs) that are represented in the figure as well. However, one of the characteristics that hinder the implementation of Zeolite 13X, is the hydrophilic characteristics of this sorbent.

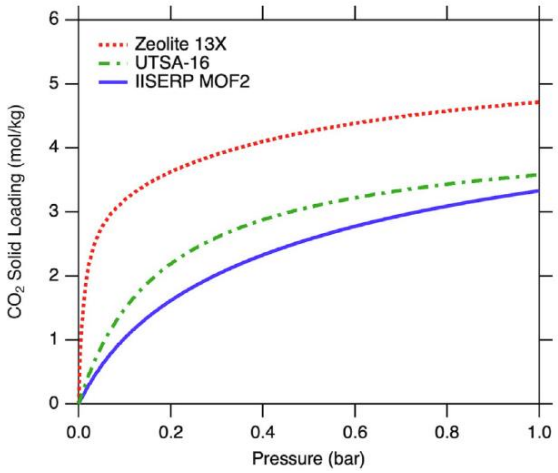

Figure 1.1: Saturation capacity of three sorbents commonly analyzed for CO_2 adsorption.[5]

The post-combustion flue generally consists of almost 10% of water content on a molar basis. When the flue gas contacts the sorbent with hydrophilic characteristics, this water content makes bound with the sorbent pores and the capacity of sorbent degrades significantly for the CO_2 adsorption. This is a such serious challenge that makes the MOFs a more promising sorbent. Although MOFs have lower saturation capacity compared to Zeolite 13X at low partial pressures, they outperform in wet environments.[8]

The selectivity of the sorbent to CO_2 compared to other components in the flue gas should be high enough to recover CO_2 from the feed stream with high purity. High CO_2 purity is essential in terms of transportation, utilization, and storage of CO_2 that should be addressed after the capture process. Although this is an important parameter in the choice of sorbent, relying too much on the selectivity of different sorbents in the sorbent screening procedures is misleading. This should not be considered as the sole parameter in order to evaluate a sorbent or the whole process scheme compared to other alternatives.[9]

The whole adsorption process is controlled kinetically. So, to develop a high-efficiency and low-cost adsorption process, the process should occur fast enough which leads to a steep breakthrough of the target component from the sorbent material and hence, a lower amount of sorbent required.[1] Thermal and mechanical stability of the sorbent are other important parameters concerning the reactor and process configuration that is implemented for the adsorption process. In Figure 1.2, the summary of important sorbent characteristics is represented.

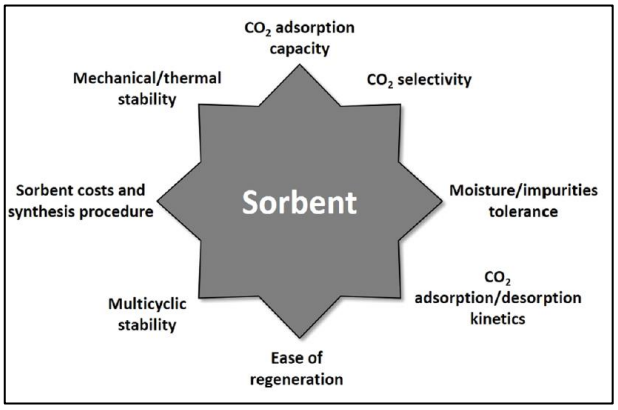

Figure 1.2: Schematic of sorbent characteristics that should be considered in adsorption system analysis.[1]

1.2. Reactor Configurations and Regeneration Strategies

To develop an adsorption process, different regeneration strategies can be implemented into different column (reactor) configurations to form the whole scheme. Two main regeneration strategies namely Temperature-Swing Adsorption (TSA) and Pressure-Swing Adsorption (PSA) utilize heat and electricity respectively to regenerate the sorbent bed.

To discuss more in detail, while adsorption is favored at low temperature and high pressure, desorption occurs by providing high temperature or low pressure which are the case for TSA and PSA respectively. Although these two are the main regeneration principals, the combination of them can be also studied in which we use the high pressure and low temperature simultaneously during the adsorption and regenerate the bed by both decreasing the pressure and increase in the temperature. This recent case leads to hybrid schemes such as TPSA or TVSA ("V" indicates that the vacuum is implemented for bed regeneration).

Different column (reactor) configurations exist that are different from each other in terms of the method that the flue gas contacts the sorbent bed. As depicted in Figure 1.3(a), in the moving bed reactor the sorbent materials move alongside the reactor after adsorbing CO_2 to be regenerated and being used in the next process cycle. The flue gas that enters the fluidized bed reactor (Figure 1.3(b)) causes the fluidization of fine sorbent particles alongside the column that is then exited from the first reactor and directed to the second one. In the second reactor, the steam is injected into the reactor and regenerates the sorbent particles for the next process cycle. This configuration is similar to the solvent-based system with a separate adsorber and regenerator acting as the absorber and stripper in such systems. However, here the

separation occurs due to the bound that formed between fine sorbent particles and CO_2 instead of the aqueous solution itself which is the case for solvent-based systems.

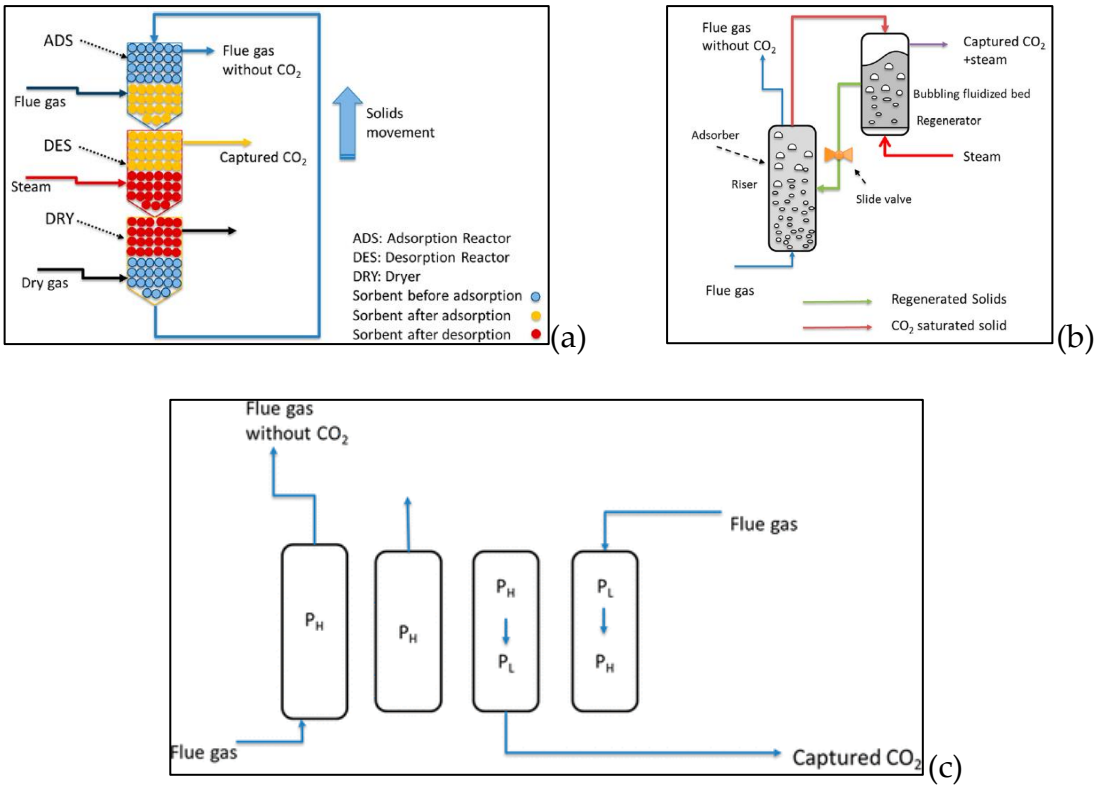

Figure 1.3: Different reactor configurations developed for post-combustion CO_2 capture: (a) Moving bed (b) Fluidized bed (c) Fixed bed.[10]

The fixed bed reactor is the most common and simplest configuration studied for post-combustion CO_2 capture. In the fixed bed reactor, the flue gas goes through the sorbent particles that are fixed in the reactor. After that the fixed sorbent bed goes through the adsorption step, the regeneration of the bed occurs without further movement of sorbent particles (Figure 1.3). An important limitation that a fixed bed reactor imposes on the system, is a higher number of columns are required to work simultaneously in different process modes. This is not the case for the other two configurations in which the movement of the sorbent materials can diminish the requirement of high column numbers.

Although all the regeneration strategies can be implemented for each reactor configuration, some of them are a good match for each other. In the next sections, we will discuss the proper reactor configuration that is suited the most for TSA and PSA regeneration strategies.

1.2.1. Temperature-Swing Adsorption (TSA)

In TSA, the bed is regenerated by applying heat to increase its temperature. At high temperature, the previously adsorbed component's bounds with the sorbent pores are gradually weakened and desorption occurs. In TSA, sorbent regeneration can be performed by direct heating. In this strategy, the sorbent bed can be purged with a hot N_2 stream or steam. Indirect heating can also be applied, where the external heating coils are integrated into the columns to provide the heat needed for bed regeneration.[1]

In the case of implementing TSA as the regeneration methodology, the type of reactor is so crucial. Fixed bed TSA requires incorporating multiple numbers of columns that work in sequence and are integrated with external heating equipment. These types of systems are not gaining attention nowadays, because of the technical complexities, high costs, and long cycle times.[11] Joss et al.[12] studied the effect of each cycle step on the main performance indicators for a fixed bed TSA system. They have analyzed four process configurations in their process modelling in which the best scenario results showed the same energy penalty compared to the benchmark MEA system for achieving purity and recovery levels of 96% and 90% respectively in the case of capturing CO_2 from post-combustion flue gas.

However, TSA processes that incorporate more complex reactor configurations are gaining more attention nowadays and are currently under development and piloting experiences. TU Wien and Shell, have cooperated in the development of a TSA configuration with a fluidized bed reactor scheme recognized as Solid Sorbent Technology (SST). The pilot plant has been developed since 2015 under the ViennaGreenCO2 project and recent results showed a steam energy demand of 3.5 MJ/kg_{CO_2} for recovery and purity levels of 90% and 95% respectively which is larger than the benchmark MEA technology.[11,13] As we can see from its process scheme in Figure 1.4(a), this is almost identical to the absorption system as two separate reactors acting individually as adsorber and desorber. In the desorber, the steam is supplied for bed regeneration which is the main source of the energy penalty.

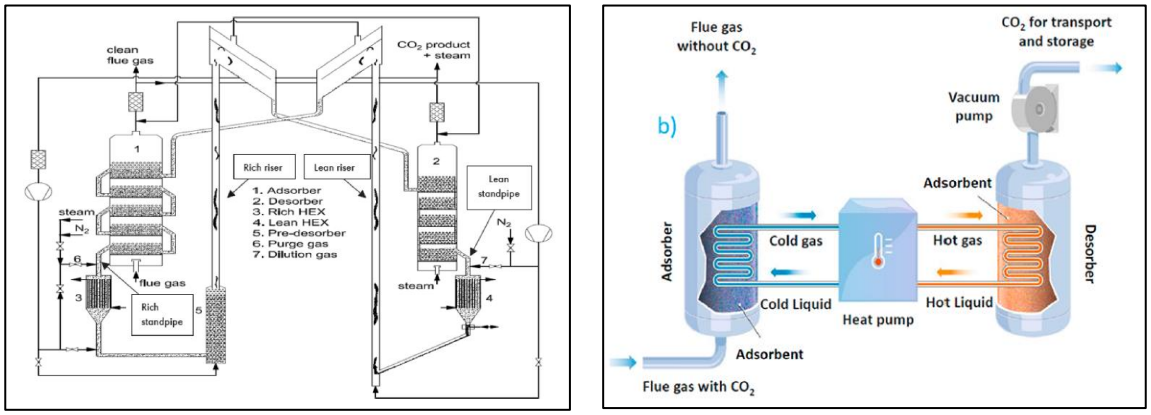

(a) (b)

Figure 1.4: Innovative TSA implementation demonstrated at pilot scale: (a) ViennaGreenCO2 pilot plant scheme[13] (b) Swing Adsorption Reactor Cluster (SARC) demonstrated at pilot scale with partial vacuum implementation (a TVSA scheme)[14]

An innovative hybrid TVSA configuration is under development by Dhoke et al.[14] which is currently being demonstrated at a lab scale known as Swing Adsorption Reactor Cluster (SARC).[15] In this configuration, the partial vacuum helps the bed regeneration which mainly occurs at high temperatures to decrease the required heat duty. Besides, the energy generated during the adsorption is recovered to be used in bed regeneration through a heat pump that works in between the two fluidized bed reactors. The process scheme is depicted in Figure 1.4(b).

1.2.2. Pressure-Swing Adsorption (PSA)

The term PSA is specifically used when the adsorption occurs at pressures above the atmospheric level and regeneration of the bed simply occurs at atmospheric pressure. In the case of implementing PSA as the regeneration strategy, the fixed-bed reactor is the only reactor studied so far. Unlike TSA, changes in reactor pressure are only applicable if we have a fixed sorbent particle in our bed. Hence, the adsorption step must be disrupted to let the bed regeneration begins. Due to this fact, we at least need two separate columns in case we aimed at continuous feed supply in a PSA adsorption system. Charles W Skarstrom, patented a 2-column, 4-step PSA scheme which can handle continuous feed that was initially developed for removing water vapor from the air.[16] However, the configuration is nowadays used in different industries such as syngas purification or separation of N_2 from the air.

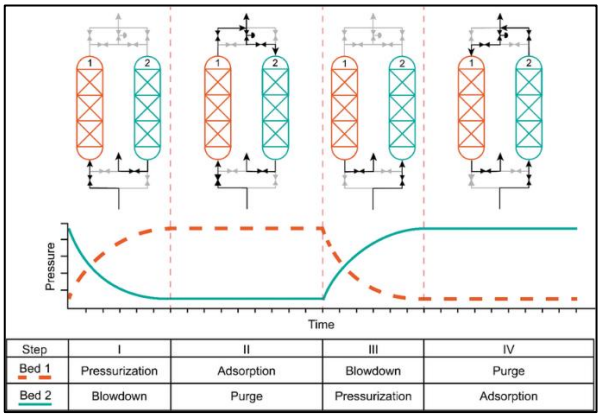

Figure 1.5: Schematic of a continuous 2-column 4-step Skarstrom cycle and the changes of pressure during each cycle step.[17]

As we can see in Figure 1.5, the process starts with pressurizing the column to a high-pressure level in which the adsorption begins. Then, the column goes through a constant-pressure adsorption step in which the main separation of the target component from the feed gas occurs. At this time, the regeneration starts in two steps. First, during the blowdown, the column pressure reaches the atmospheric pressure by removing the remained gas from the column. Then, the column is purged with gas at atmospheric pressure to both regenerate the bed and extract the captured component. We can also see from this figure, the sequence of steps in the two columns required for a continuous capture system.

The 4-step that indicated in Figure 1.5 is the minimum steps that are required to be implemented in a PSA adsorption system. The Skarstrom cycle is so general, meaning that it can be implemented for any type of gas separation application that is needed. However, the peculiarities of each process and the objective that we are followed play an important role to modify the sequence of steps and the steps themselves as well. For instance, in the case of post-combustion CO_2 capture, the target adsorbate is CO_2 and we expect very high recovery from the whole scheme. So, researchers suggested adding further cycle steps to the basic one. While some strategies such as "pressure equalization" and "evacuation" are pursuing the same target as in the blowdown to decrease the pressure of the column, others such as "rinse" aimed at regeneration the bed and recovering the target component with high purity at expense of higher energy consumption.

According to the knowledge of the author, Liu et al.[18] were the pioneer research group that designed and modeled three specific PSA (as a vacuum is partially implemented in their proposed process, the term VPSA is used) adsorption systems for CO_2 capture from a coal-fired power plant's flue gas. The best configuration, namely the 2-stage 5-column cycle using Zeolite 13X in the first stage and Activated Carbon in the second stage sorbent material. The performance of this configuration

is reported as the power consumption of 0.756 MJ/kg_{CO_2} for the recovery and purity levels of 90% and 95% respectively.

They have reported for achieving these levels of recovery and purity, implementing pressure equalization and rinse step is inevitable which ultimately resulted in a complex cycle in terms of columns schedule and timing. This research group also demonstrated this configuration at a pilot scale[19], in which for the same levels of purity and recovery, they reported energy consumption of 2.44 MJ/kg_{CO_2} which is way higher than the results they previously obtained from process simulation.

Riboldi et al.[3] studied the same configuration for a large-scale coal-fired power plant. They reported that although implementing such a process resulted in slightly lower energy consumption compared to the benchmark amine technology, it ultimately resulted in a very large footprint, due to the large number of columns that should be implemented for treating the total amount of flue gas and the scenario would be unlikely to be feasible for further development.

Table 1.1: Performance of recognized pilot scale sorbent-based CO_2 capture.

Flue Gas Source	Sorbent	Type	Pilot Size $\left[\frac{m_n^3}{h}\right]$	$\%mol\ CO_2$	Recovery	Purity	Energy Consumption $\left[\frac{MJ_{el}}{kg_{CO_2}}\right]$	Ref.
62.5 MW_{th} Biomass CHP plant	Amine functionalized	TSA	670	2.5%	N.A.	N.A.	1.80[i]	[13]
460 MW_{th} Coal-fired boiler	AC	PSA	100	14.0%	44.6%	87.5%	3.52	[20]
Coal-fired power plant	Zeolite 13X + AC	PSA	35	16.5%	90.2%	95.6%	2.44	[19]

Data and performance of 3 pilot scale works are reported in Table 1.1. Although in the first insight, the sorbent-based systems outperform the solvent-based systems in terms of lower energy penalty, the results from pilot experiences showed higher energy consumption compared to the process simulation results. It is of crucial importance to evaluate all the systems on the same basis. For instance, the energy consumption reported from the ViennaGreenCO2 project[13] (Figure 1.4(a)) is related to the feed gas containing only 2.5% of CO_2. Besides, the transformation of thermal energy into electricity is important if we aimed at comparing TSA to PSA systems. This transformation is taken into account in the results reported in Table 1.1.

Compared to the typical value of $2.5 - 4\ MJ_{th}/kg_{CO_2}$ as the thermal energy needed in the reboiler for solvent regeneration in a solvent-based capture system,

[i] Transformation of thermal energy to electrical energy is considered by a factor of 1/3.

performances of all the pilot schemes showed higher energy consumption. This issue will be further discussed in the next section.

1.3. Vacuum-Swing Adsorption (VSA)

Vacuum-Swing Adsorption (VSA) follows the same principle as the PSA, in which the main difference is that the maximum pressure that the adsorption occurs is fixed at the atmospheric level. This is an interesting option in the case of CO_2 capture from post-combustion flue gas that discharged from the stack at around atmospheric pressure. Although in such a scheme, the compression work is not necessary for preparing the gas in the adsorption step, vacuum pumps are used to provide sub-atmospheric pressure levels in the column, which favors the desorption of adsorbate (CO_2 in our case) during the regeneration steps.

There are plenty of studies that developed a VSA scheme for post-combustion CO_2 capture.[4,6,21,22] Among them, Haghpanah et al.[4] aimed to develop a modeling and optimization framework for a 4-step VSA cycle. This cycle is a resemblance to the Skarstrom cycle, with the main difference of incorporating another evacuation step in addition to blowdown, to extract the adsorbed CO_2 from the column. This step is replaced the purge step due to the inherent of the VSA scheme in which purge of the bed at atmospheric pressure cannot be implemented and regeneration of the bed should be performed under vacuum conditions. They compared 7 different configurations among which, the 4-step cycle with Light Product Pressurization (LPP) is reported as the best scenario. For this scheme, the energy consumption for 95% of purity and 90% of recovery is reported to be 154 kWh/t_{CO_2}.[23] This is the equivalent of 0.554 MJ_{el}/kg_{CO_2} and compared to the values reported in Table 1.1, it shows promising results in terms of energy consumption.

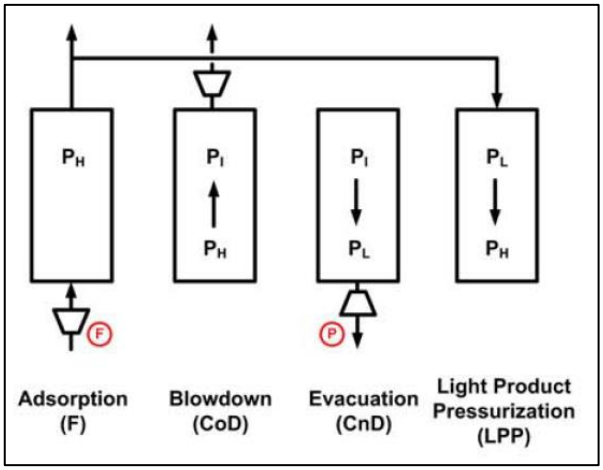

Figure 1.6: 4-step VSA cycle with LPP studied by Haghpanah et al.[23] Process steps and sequence.

This configuration is demonstrated at the pilot scale by Krishnamurthy et al.[24] In this pilot, a binary mixture of $15\%_{vol}$ CO_2 and $85\%_{vol}$ N_2 is fed into the system as a simplified dried flue gas. For the same levels of purity and recovery, they measured the energy consumption of 510.5 kWh/t_{CO_2} ($= 1.83\ MJ_{el}/kg_{CO_2}$) which is almost 3 times higher than the values reported from process simulations previously.

The main assumption in the process simulation that causes this difference is reported to be the vacuum pump efficiency. A typical value of 72% in considered for the vacuum pump efficiency. However, to make the process simulation compatible with the measured data a pump efficiency of 30% should be taken into account. This is because of the fact that vacuum pump efficiency decreases exponentially for providing the very low vacuum levels that we need in the VSA systems. They also tested multiple numbers of vacuum pumps to see the effect of the pressure on the efficiency which is depicted in Figure 1.7.

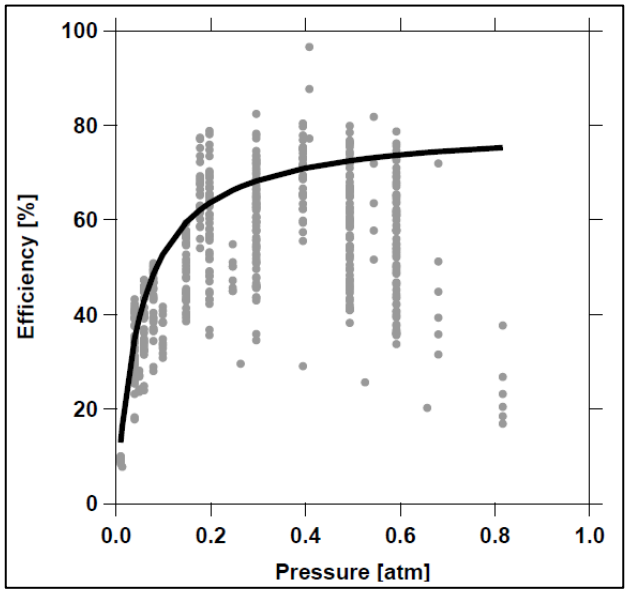

Figure 1.7: Vacuum pump efficiency as a function of operating pressure. The dots represented the measured data from different vacuum pumps and the line is the fitted curve for which the modeling equation is obtained.[25]

In Figure 1.7, it has shown that for providing pressures lower than 0.2 atm, which is the case for both the blowdown and evacuation steps, the pump efficiency drops significantly to below 30%, and the energy consumption increases. This is an important issue to be considered while studying the VSA scheme and process scale-up strategies. Otherwise, the calculated energy consumption would be misleading.

1.4. Remarks and Important Understandings

I. In analyzing the sorbent-based capture systems, it is important to evaluate the energy consumption on the same basis (thermal or electrical). This is important, especially in the PSA schemes where electricity is used. The conversion of 30% for the transformation of thermal energy into electricity is an acceptable assumption. As a result, the comparison of PSA to either the TSA system or the benchmark amine technologies in which energy penalty is always reported based on thermal energy consumption would be reasonable.

II. Experimental studies showed a significant drop in the vacuum pump efficiency at low vacuum pressures. In case of implementing VSA or even TVSA schemes, for a more realistic vacuum pump energy consumption, studies such as the one reported in Figure 1.7 is necessary which suggests the drop of the efficiency to around 30% for low vacuum levels instead of typical efficiency assumption of 70% that is assumed by the vast majority of studies in this field.

For instance, Jiang et al.[2] compared three sorbent-based schemes for CO_2 capture without considering the effects we discussed in previous point. The energy consumption of the VPSA cycle is reported to be way lower than the other two schemes (Figure 1.8(a)). The more accurate representation of the figure to avoid misleading information is to assess all the schemes based on thermal energy consumption (Figure 1.8(b)), as well as taking into account the decreased efficiency of the vacuum pump (Figure 1.8(c)).

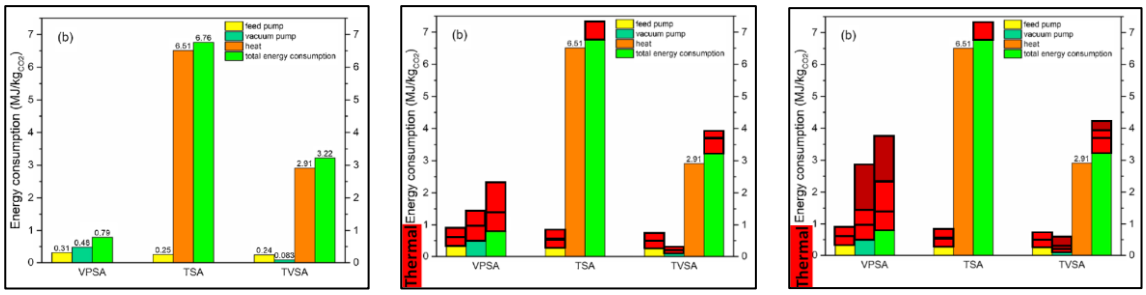

(a) (b) (c)

Figure 1.8: Energy consumption (a) Reported by Jiang et al.[2] (b) Taking into account the transformation of thermal energy to electricity (light red) (c) Considering the decrease in vacuum pump efficiency (dark red).

By doing the transformation, the VPSA system still outperforms the other two schemes in terms of energy consumption. However, the difference is not as significant as the one reported initially.

III. In most studies, the simplified gas mixture of $15\%_{vol}$ CO_2 and $85\%_{vol}$ N_2 is considered a representative of real flue gas. However, in the real case, the water content of the flue gas imposes serious limitations on choosing the proper sorbent material. Besides, the partial pressure of CO_2 varies in flue gases based on the composition and characteristics of the fuel used in the host plant. This can affect the cost significantly such that Subraveti et el.[26] reported that for the imaginary zero-cost adsorbent, the cost of CO_2 avoided for PVSA schemes ranges from 87.1 to 10.4 $\frac{€}{t_{CO_2,avoided}}$ corresponding to CO_2 molar fraction in the feed gas varies from $3.5\%_{vol}$ to $30\%_{vol}$.

IV. Other uncertainties such as implementing the valve equation in calculating the dynamic operation of columns or other simplifying assumptions that can be used in the process modeling such as neglecting pressure drop alongside the column or isothermal adsorption process should be taken into account. As this process is not mature enough for post-combustion CO_2 capture, these uncertainties can have a significant effect on the performance of the system on a large scale.

2 VSA Process Modelling

2.1. Model Equations

2.1.1. Component Mass Balance

To model each step of an adsorption/desorption system, we mainly need to consider a proper mass balance equation that defines the balance of mass over time. This can be coupled with the momentum balance equation for evaluating the effect of pressure drop and changes in velocity caused by pressure drop alongside the column.

Furthermore, the energy balance equation can be implemented to estimate the temperature changes due to the heat that generates or disappear in the column during the adsorption and desorption steps, respectively.

The process inside the column can be modeled as a plug, that moves toward the column. Considering the assumptions of the axially dispersed plug flow model, we can write the mass balance equation inside the column for component "i" in the following form:

$$\underset{\text{(i)}}{\varepsilon_b \frac{\partial C_i}{\partial t}} = \underset{\text{(ii)}}{-(1-\varepsilon_b)\rho_s \frac{\partial q_i}{\partial t}} \underset{\text{(iii)}}{- \varepsilon_b \frac{\partial (uC_i)}{\partial z}} + \underset{\text{(iv)}}{\varepsilon_b \frac{\partial}{\partial z}\left(D_L \frac{\partial C_i}{\partial z}\right)} \tag{2.1}$$

To briefly describe each term of equation (2.1), we can say:

- **(i): Accumulation term;** which shows the accumulation of component "i" in the gas phase over time.
- **(ii): Generation term;** which is the representative of the mass transfer from the gas into the solid (or vice versa) over time.
- **(iii): Convection term;** which shows the movement of component "i" in the bulk gas w.r.t first order spatial derivative.
- **(iv): Diffusion term;** which shows the movement of component "i" in the bulk gas w.r.t second-order spatial derivative.

Equation (2.1), has two important peculiarities related to the bed voidage contributions on each term that are important to be rightly interpreted to avoid any confusion:

Firstly, the concentration of component "i" in the gas and solid are referred to the different volume basis:

$$C_i = \frac{N_i^{gas}}{V_{voidage}} \tag{2.2}$$

$$q_i = \frac{N_i^{solid}}{V_{sorbent}} \tag{2.3}$$

So, in order to be able of including both of these concentrations in one equation, we need to normalize the referenced volume referring to the volume of the column. This is done by implementing a proper constant for each term based on the bed voidage. For the gas phase, we can write:

$$\frac{N_i^{gas}}{V_{column}} = \frac{V_{voidage}}{V_{column}} \times \frac{N_i^{gas}}{V_{voidage}} \tag{2.4a}$$

$$\frac{N_i^{gas}}{V_{column}} = \varepsilon_b C_i \tag{2.4b}$$

Similarly, we can write the below equations for the solid phase:

$$\frac{N_i^{solid}}{V_{column}} = \frac{V_{sorbent}}{V_{column}} \times \frac{N_i^{solid}}{V_{sorbent}} \tag{2.5a}$$

$$\frac{N_i^{solid}}{V_{column}} = (1 - \varepsilon_b) q_i \tag{2.5b}$$

Secondly, another important consideration is the difference between the superficial gas velocity and interstitial gas velocity. Superficial gas velocity is the velocity through which the gas moves toward an empty column. Interstitial gas velocity is the actual velocity of gas inside the column considering the presence of solid sorbent particles. So, considering a constant volume flow rate of gas, the relation between these two velocities can be written as:

$$A_{eff} \times u_{interstitial} = A_{column} \times v_{superficial} \tag{2.6a}$$

$$A_{eff} = A_{column} \times \varepsilon_b \tag{2.6b}$$

$$u_{interstitial} = \frac{v_{superficial}}{\varepsilon_b} \tag{2.6c}$$

In fact, it represents the increase of superficial velocity that happens due to the lower space that gas can move through because of the presence of solid sorbent particles. So, if we want to write equation (2.1), based on the superficial velocity, we should consider this transformation of velocity.

Considering equation (2.2) and assuming ideal behavior for the gas phase, we can derive gas phase concentration from ideal gas law as:

$$C_i = y_i \frac{p}{RT} \tag{2.7}$$

2.1.2. Mass Transfer

To evaluate the amount of each gas component adsorbed in the solid, we need to model a mass transfer process. Two approaches are investigated in this study as below.

Instantaneous Equilibrium

In an ideal condition, each component in the gas mixture is instantaneously reached its saturation capacity at the working condition. Hence, we can write:

$$\frac{\partial q_i}{\partial t} = \frac{\partial q_i^*}{\partial t} \tag{2.8}$$

To evaluate the saturation capacity, we should use a model to describe the saturation capacity at each partial pressure of gas component at a constant temperature which is called the adsorption isotherm. As we are dealing with a binary gas mixture in our case, a model which can simultaneously consider the effect of gas phase composition, as well as total gas pressure, is Dual-site Extended Langmuir model.

"Dual-site" is more accurate compared to the "Single-site" model which can take into account more available adsorption sites. Besides, "Extended" means that the model is considering the binary interactions of the components in the mixture.

Haghpanah et al. gravimetrically measured the equilibrium data of Carbon dioxide and Nitrogen binary mixture on Zeolite 13X, which is fitted to the Dual-site Extended Langmuir model as below: [4]

$$q_i^* = \frac{q_{sb,i}\, b_i\, C_i}{1 + \sum b_i C_i} + \frac{q_{sd,i}\, d_i\, C_i}{1 + \sum d_i C_i} \tag{2.9}$$

Where $q_{sb,i}$ and $q_{sd,i}$ are solid phase saturation loadings.(in $[\frac{mol}{kg}]$) and b_i and d_i are Arrhenius type temperature dependence (in $[\frac{m^3}{mol}]$). The Arrhenius type temperature dependency terms can be obtained as:

$$b_i = b_{0,i}\, exp\left(-\frac{\Delta U_{b,i}}{RT}\right) \tag{2.10a}$$

$$d_i = d_{0,i}\, exp\left(-\frac{\Delta U_{d,i}}{RT}\right) \tag{2.10b}$$

The parameters for the calculation of adsorption isotherms are shown in Table 2.1 as below:

Table 2.1: Isotherm parameters of CO_2 and N_2 mixture on Zeolite [4].

$\boldsymbol{Parameter}$	$\boldsymbol{CO_2}$	$\boldsymbol{N_2}$
$\boldsymbol{b_0\ [m^3/mol]}$	8.65×10^{-7}	2.5×10^{-6}
$\boldsymbol{d_0\ [m^3/mol]}$	2.63×10^{-8}	0
$\boldsymbol{\Delta U_{b,i}[J/mol]}$	-36641.21	-1.58×10^4
$\boldsymbol{\Delta U_{d,i}[J/mol]}$	-35690.66	0
$\boldsymbol{q_{sb,i}\ [mol/kg]}$	3.09	5.84
$\boldsymbol{q_{sd,i}\ [mol/kg]}$	2.54	0

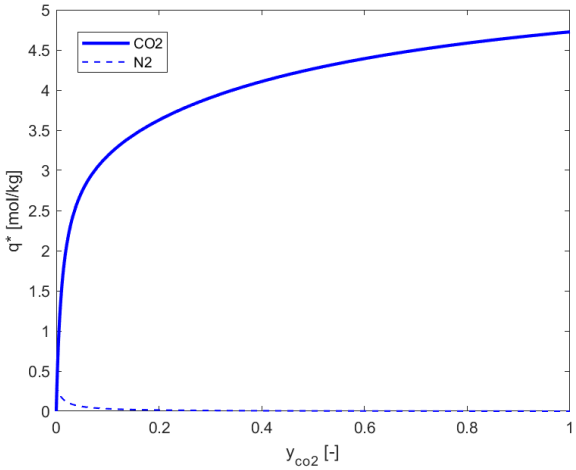

Figure 2.1: Dual-site Extended Langmuir Isotherms for CO_2 and N_2 at 1 bar, 298K on Zeolite 13X.

In Figure 2.1, adsorption isotherms for both CO_2 and N_2 are obtained for the total gas pressure of 1 bar and temperature of $298K$. From Figure 2.1, it can be seen that the selectivity of Zeolite 13X is higher for adsorption of CO_2 over N_2. When the gas is rich in N_2, the saturation capacity of N_2 is higher than of CO_2. However, when the gas becomes richer in $CO2$, due to this higher selectivity, The saturation capacity of N_2 is decreasing exponentially and most sites are available for the CO_2 adsorption. This is one of the main reasons that Zeolite 13X can be considered a good sorbent for CO_2 capture. In Figure 2.2, we can see the variation of saturation capacity for both components at three pressure levels w.r.t. changes of CO_2 molar fraction in the gas mixture.

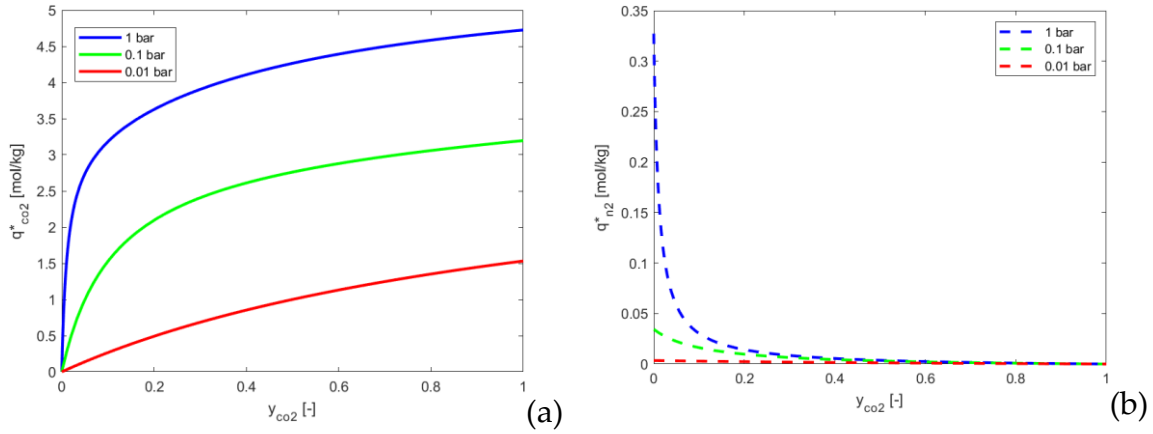

Figure 2.2: Dual-site Extended Langmuir Isotherms of Zeolite 13X for three levels of total gas pressure for (a) CO_2 and (b) N_2 at 298K.

Linear Driving Force (LDF)

Moving forward to the reality from the ideal equilibrium assumption, different resistances avoid the solid sorbent to reach instantaneous equilibrium. 3 main resistances are:

- Gas film resistance
- Macropore resistance
- Micropore resistance

In the LDF model, we can consider that **Macropore resistance** is the dominant term that defines the mass transfer rate. This is the case that can model the behavior of CO_2/N_2 mixture adsorption on Zeolite 13X.[4]

The rate of adsorption of gas in the solid, using the LDF model can be written as:

$$\frac{\partial q_i}{\partial t} = k_{LDF,i}(q_i^* - q_i) \tag{2.11}$$

Where $k_{LDF,i}$ is the mass transfer resistance of the LDF model which is defined as:

$$k_{LDF,i} = 15\frac{D_{e,i}}{r_p^2} \tag{2.12}$$

Effective gas diffusivity depends on both the characteristics of the sorbent itself, as well as the equilibrium isotherm of each component which is defined in the previous part, using the Dual-site Extended Langmuir model. So, it is important to consider that the mass transfer coefficient is changed by any changes in the **sorbent**, the **operating conditions**, and **the gas mixture**. The correlation to calculate this effective gas diffusivity is:

$$D_{e,i} = \frac{\varepsilon_P D_P}{K_i} \tag{2.13}$$

From the parameters in equation (2.13), ε_p and D_p are the sole characteristics of the **sorbent**, while K_i depends on the **operating conditions** and **the gas mixture**. Effective macropore diffusivity can be obtained using the following correlation:

$$D_p = \frac{D_m}{\tau} \tag{2.14}$$

Molecular diffusivity is a representative of the combined effect of **Knudsen** and **Viscous** diffusivity. Considering the effect of K_i in the mass transfer coefficient which can be obtained from relevant isotherms in Figure 2.1, we can expect a lower mass transfer coefficient at a lower CO_2 concentrations, while it becomes higher when the gas phase is concentrated in CO_2.

2.2. Solution Methodology

Before solving the mass balance equation, we have implemented further simplifying assumptions. The complete list of assumptions is given below:

- The axially dispersed plug flow model is used to model the bulk gas flow inside the column.
- The gas phase behavior is assumed to be ideal.
- Dual-site Extended Langmuir model is used for the calculation of the saturation capacity of gas in the solid sorbent.

- Linear Driving Force (LDF) model is used for the mass transfer.
- Neglecting diffusion term.
- No gradients of concentration in the radial direction.
- No pressure drop inside the column.
- Isothermal adsorption process.
- Uniform sorbent properties alongside the column.

Considering the above-mentioned assumptions and from equations (2.1), (2.7), and (2.11), we can rewrite the component mass balance equation in the below form:

$$\frac{\partial y_i}{\partial t} + \frac{y_i}{p}\frac{\partial p}{\partial t} = -\frac{RT}{p}\frac{1-\varepsilon_b}{\varepsilon_b}\rho_s \frac{\partial q_i}{\partial t} - y_i \frac{\partial u}{\partial z} - u\frac{\partial y_i}{\partial z} \tag{2.15}$$

As we are dealing with a binary gas mixture, the summation of molar fractions of CO_2 and N_2 for each step at every time is 1. So we can write:

$$y_{CO_2} + y_{N_2} = 1 \tag{2.16a}$$

$$y_{N_2} = 1 - y_{CO_2} \tag{2.16b}$$

Now we can apply the component mass balance from equation (2.15) to both components in our gas mixture, namely CO_2 and N_2. For CO_2, we can write it as:

$$\frac{\partial y_{CO_2}}{\partial t} + \frac{y_{CO_2}}{p}\frac{\partial p}{\partial t} = -\frac{RT}{p}\frac{1-\varepsilon_b}{\varepsilon_b}\rho_s \frac{\partial q_{CO_2}}{\partial t} - y_{CO_2} \frac{\partial u}{\partial z} - u\frac{\partial y_{CO_2}}{\partial z} \tag{2.17}$$

For N_2, we can combine the two equations of (2.15) and **Error! Reference source not found.** which results in:

$$-\frac{\partial y_{CO_2}}{\partial t} + \frac{1}{p}\frac{\partial p}{\partial t} - \frac{y_{CO_2}}{p}\frac{\partial p}{\partial t} = -\frac{RT}{p}\frac{1-\varepsilon_b}{\varepsilon_b}\rho_s \frac{\partial q_{N_2}}{\partial t} - \frac{\partial u}{\partial z} + y_{CO_2}\frac{\partial u}{\partial z} + u\frac{\partial y_{CO_2}}{\partial z} \tag{2.18}$$

Summing up the equations (2.17) and (2.18), we will have:

$$\frac{\partial u}{\partial z} = -\frac{RT}{p}\frac{1-\varepsilon_b}{\varepsilon_b}\rho_s \sum \frac{\partial q_i}{\partial t} - \frac{1}{p}\frac{\partial p}{\partial t} \tag{2.19}$$

Replacing $\frac{\partial u}{\partial z}$ in equation (2.17) with correlation we obtained in (2.19), results in:

$$\frac{\partial y_{CO_2}}{\partial t} = -\frac{RT}{p}\frac{1-\varepsilon_b}{\varepsilon_b}\rho_s \left(\frac{\partial q_{CO_2}}{\partial t} - y_{CO_2}\sum \frac{\partial q_i}{\partial t}\right) - u\frac{\partial y_{CO_2}}{\partial z} \tag{2.20}$$

In general, the main unknowns in equations (2.19) and (2.20) are y_{CO_2} and u.

2.2.1. Composition Calculation

As we are dealing with a Partial Differential and Algebraic Equation (PDAE) here which is distributed over time (t) and space (z), we should use a numerical solution approach to solve it.

The first option is to completely discretize y_{CO_2} over both time and space. Alternatively, we can only discretize it over space using the **Method of Lines (MoL)** and converting it to a set of Differential Algebraic Equations (DAEs). Then, these sets of DAEs can be integrated over time by using a standard integration method. This can be done by various MATLAB solver algorithms such as **ode15s**.

To discretize the y_{CO2} over space, first, we need to divide the column into a finite number of slices. As we can see in Figure 2.3, considering the column with the length of L is dividing into N slices, then we have $N + 1$ walls for each we should implement the mass balance equation.

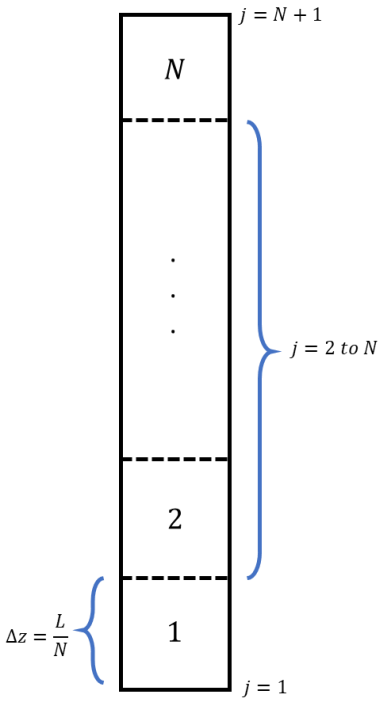

Figure 2.3: Splitting column into a finite number of slices.

Using the backward approach from the MoL, we can write the derivative of y_{CO_2} over space in the following form:

$$\frac{\partial y_{CO_2,1}}{\partial z} = \frac{y_{CO_2,1} - y_{CO_2,0}}{\Delta z} \; for\; j = 1 \tag{2.21}$$

$$\frac{\partial y_{CO_2,j}}{\partial z} = \frac{y_{CO_2,j} - y_{CO_2,j-1}}{\Delta z} \; for\; j = 2\; to\; N+1 \tag{2.22}$$

The reason that we have separated the first wall is that by using the backward approach, we need to define an artificial term of $y_{CO_2,0}$. Based on the boundary condition at each step, we should impose suitable constraints for this term that will be discussed in the relevant section.

Thanks to this semi-discretization approach, we can now define systems of DAEs that only consist of derivatives in the time domain. From equation (2.20) we can now write:

$$\frac{\partial y_{CO_2,j}}{\partial t} = -\frac{RT}{p}\frac{1-\varepsilon_b}{\varepsilon_b}\rho_s\left(\frac{\partial q_{CO_2,j}}{\partial t} - y_{CO_2,j}\sum\frac{\partial q_{i,j}}{\partial t}\right) - u_j\frac{y_{CO_2,j} - y_{CO_2,j-1}}{\Delta z} \quad j = 1, \dots, N+1 \tag{2.23}$$

This equation at each wall should be coupled with equation (2.11) which determines the rate of adsorption of gas in the solid. Re-writing equation (2.11) for each wall, results in:

$$\frac{\partial q_{i,j}}{\partial t} = k_{LDF,i}\left(q^*_{i,j} - q_{i,j}\right) \qquad j = 1, \dots, N+1 \tag{2.24}$$

As the saturation capacity can be intercepted as a function of y_{CO_2}, equations (2.23) and (2.24) can be numerically solved at the same time, over the time domain for the calculation of y_{CO_2}.

To summarize, we have 3 systems of equations that should be solved simultaneously to obtain y_{CO_2} in the below form:

$$\begin{bmatrix} \frac{\partial q_{CO_2,1}}{\partial t} \\ \vdots \\ \frac{\partial q_{CO_2,N+1}}{\partial t} \end{bmatrix} = k_{LDF,CO_2} \times \begin{bmatrix} q^*_{CO_2,1} - q_{CO_2,1} \\ \vdots \\ q^*_{CO_2,N+1} - q_{CO_2,N+1} \end{bmatrix} \tag{2.25}$$

$$\begin{bmatrix} \frac{\partial q_{N_2,1}}{\partial t} \\ \vdots \\ \frac{\partial q_{N_2,N+1}}{\partial t} \end{bmatrix} = k_{LDF,N_2} \times \begin{bmatrix} q^*_{N_2,1} - q_{N_2,1} \\ \vdots \\ q^*_{N_2,N+1} - q_{N_2,N+1} \end{bmatrix} \tag{2.26}$$

$$\begin{bmatrix} \frac{\partial y_{CO_2,1}}{\partial t} \\ \vdots \\ \frac{\partial y_{CO_2,N+1}}{\partial t} \end{bmatrix} = -\frac{RT}{p}\frac{1-\varepsilon_b}{\varepsilon_b}\rho_s \times \begin{bmatrix} \frac{\partial q_{CO_2,1}}{\partial t} - y_{CO_2,1}\sum\frac{\partial q_{i,1}}{\partial t} \\ \vdots \\ \frac{\partial q_{CO_2,N+1}}{\partial t} - y_{CO_2,N+1}\sum\frac{\partial q_{i,N+1}}{\partial t} \end{bmatrix} - [u_1 \quad \dots \quad u_{N+1}] \times \begin{bmatrix} \frac{y_{CO_2,1}-y_{CO_2,0}}{\Delta z} \\ \vdots \\ \frac{y_{CO_2,N+1}-y_{CO_2,N}}{\Delta z} \end{bmatrix} \tag{2.27}$$

2.2.2. Velocity Calculation

Another unknown in the mass balance equation is the velocity through which the gas moves through the column. This velocity which represents the flow rate of each gas component, changes over time based on the transfer of mass from the gas into the solid (or vice-versa).

Hence, we must define a method to update the velocity field after each time step and implement the updated value in equation (2.27) for the next time step. To do so, we can discretize u over space using the same approach that we performed for y_{CO_2} and re-write (2.19) in the discretized form as below:

$$\frac{u_j - u_{j-1}}{\Delta z} = -\frac{RT}{p}\frac{1-\varepsilon_b}{\varepsilon_b}\rho_s\sum\frac{\partial q_{i,j}}{\partial t} - \frac{1}{p}\frac{\partial p}{\partial t} \tag{2.28}$$

The changes in pressure over time for pressure-changing steps are given as an input to solve the equation (2.28). Considering the functional form proposed by Chue et al.[27], we can use the following equation to simulate the pressure profile over time:

$$\begin{cases} p(t) = C_0 + C_1 e^{-C_2 t} \\ where: \\ C_0 = a \times p_f \\ C_1 = p_0 - a \times p_f \\ C_2 = \dfrac{-\ln\left[(1-a)/(\gamma - a)\right]}{t_f} \end{cases} \tag{2.29}$$

In which the pressure changes from p_0 to the final value of p_f and γ is the ratio of p_0 to p_f for a time step from 0 to t_f. The values of coefficient a are 1.1 for pressure-increasing steps and 0.9 for pressure-reduction steps.

The main reason behind using the above-mentioned functional form for the pressure changing step is that in such steps, the pressurization (or depressurization) rate is initially high due to the relatively large pressure difference. As the pressure difference gradually becomes smaller, this rate will be decreased simultaneously. This behavior can be well-simulated by such exponential correlation.

To briefly discuss the solution procedure, we can consider the first time step as $t = [0,1]$. Then, by assuming that the velocity field is initially 0 at each slice wall (or we

can define it based on implemented boundary conditions), first, we can solve the system of equations (2.25) to (2.27) simultaneously. Then, by calculating $\frac{\partial q_i}{\partial t}$ for each component at each wall, we can update the velocity at each wall by using equation (2.28). These updated values will be used in the next time step for the calculation of y_{CO_2} at each slice wall.

2.3. Cyclic Process

A cyclic pressure swing adsorption process consists of different steps. Such processes start with pressurization of the column to provide the high pressure that the adsorption process requires. Then, feed is continuously supplied to the column at a pre-determined rate and the target component is adsorbed in the sorbent.

After the adsorption step is completed, we need to depressurize the column to regenerate the sorbent bed and make it ready for the next cycle. Here, there are different options such as co-current/counter-current blowdown and pressure equalization. The choice of implementing different depressurization strategies is a matter of design considering the operating conditions, target performance (such as a certain level of purity, recovery, or energy consumption), and plant costs.

Other steps such as purge and rinse can be included in the cyclic steps. The main aim of including such processes is to increase purity or recovery at the expense of higher energy consumption.

2.3.1. 4-step Cyclic VSA Process

In this work, we consider a basic 4-step vacuum swing adsorption process which is also studied by a number of authors for the separation of CO_2 from CO_2/N_2 gas mixture as a representative of dry flue gas. [4,24,28]. Process steps are described below:

Pressurization (P): The column is pressurized to a high-pressure level (p_H) which is 1 bar in the case of the VSA process. At this step, the feed end of the column is opened and the product end is closed until we reach p_H inside the column

Adsorption (A): Feed gas is supplied to the column from the feed end at a predetermined rate. At this step, the component with higher selectivity (i.e. CO_2) is preferentially adsorbed into the sorbent bed and component with lower selectivity (i.e. N_2) is released from the product end of the column which is open during this adsorption step.

Co-current blowdown (B): By performing evacuation to the product end of the column at this step while the feed end is closed, we aim at decreasing the column

pressure to the intermediate pressure level (p_I). So, we preferentially extract the remaining N_2 that exists in the column from the previous step (either in the gas phase or solid phase).

Counter-current evacuation (E): Similar to the previous step, we perform evacuation to decrease the pressure of the column to a low-pressure level (p_L). The main target at this step is to recover the captured CO_2. So, we perform evacuation at the feed end of the column while the product end is closed. Consequently, the CO_2 which is concentrated in the first half of the column will be preferentially desorbed and extracted to be further purified, or for direct utilization and storage.

In Figure 2.4, we can see the above-mentioned steps together with the column feed and product ends condition in each step.

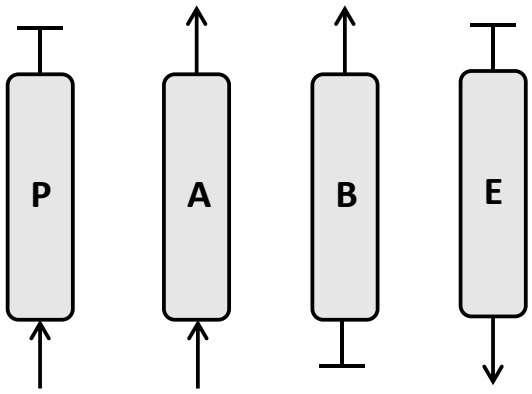

Figure 2.4: Schematic of a 4-step VSA cycle.

To model the phenomena that occur in each step in terms of mass balance, we must solve the system of equations (2.25) to (2.27) and (2.28) for each step considering proper boundary conditions which impose the feed and product end conditions in the model. Considering the discretized scheme in Figure 2.3, proper boundary conditions can be written as in Table 2.2:

Table 2.2: Boundary conditions for each step.

	Pressurization (P)	Adsorption (A)	Blowdown (B)	Evacuation (E)
Feed end B.C.	$y_{CO_2,1} = y_{CO_2,feed}$	$\begin{cases} y_{CO_2,1} = y_{CO_2,feed} \\ u_1 = u_{feed} \end{cases}$	$\begin{cases} \frac{\partial y_{CO_2,1}}{\partial z} = 0 \\ u_1 = 0 \end{cases}$	$\frac{\partial y_{CO_2,1}}{\partial z} = 0$
Product end B.C.	$\begin{cases} \frac{\partial y_{CO_2,N+1}}{\partial z} = 0 \\ u_{N+1} = 0 \end{cases}$	$\frac{\partial y_{CO_2,N+1}}{\partial z} = 0$	$\frac{\partial y_{CO_2,N+1}}{\partial z} = 0$	$\begin{cases} \frac{\partial y_{CO_2,N+1}}{\partial z} = 0 \\ u_{N+1} = 0 \end{cases}$

2.3.2. Performance Indicators

To evaluate the performance of the Carbon capture systems, there is a number of performance indicators that makes us able to not only evaluate the performance of a developed system itself but also compare different capture systems on the same basis. Purity, recovery, and specific energy consumption are among the most important ones. In this work, we have defined them based on the inherent of the model as:

$$Purity = \frac{N_F^{CO2}|_E}{N_F^{tot}|_E} \tag{2.30}$$

$$Recovery = \frac{N_F^{CO2}|_E}{N_F^{CO2}|_P + N_F^{CO2}|_A} \tag{2.31}$$

Where $N_F^{CO2}|_E$ and $N_F^{tot}|_E$ indicates the moles of CO_2 and the total number of moles that exits from the feed end during the evacuation period, respectively. They can be defined as follows:

$$N_F^{CO2}|_E = \frac{A_{eff}}{RT} \times \int_0^{t_E} p(t).u(t).y_{CO2}(t).dt \tag{2.32}$$

$$N_F^{tot}|_E = \frac{A_{eff}}{RT} \times \int_0^{t_E} p(t).u(t).dt \tag{2.33}$$

Similar to $N_F^{CO2}|_E$, we can define $N_F^{CO2}|_P$ and $N_F^{CO2}|_A$ which are the moles of CO_2 that enters the column from the feed end during the pressurization and adsorption steps, respectively.

$$N_F^{CO2}|_P = \frac{A_{eff}}{RT} \times \int_0^{t_P} p(t).u(t).y_{CO2}(t).dt \tag{2.34}$$

$$N_F^{CO2}|_A = \frac{A_{eff}}{RT} \times \int_0^{t_A} p_H.u_{feed}.y_{CO2,feed}.dt \tag{2.35}$$

It is worth mentioning that as in the pressurization and evacuation steps, pressure, velocity, and composition are changing continuously over time, we must perform the integration over time. However, as we can see in the equation (2.35), during the adsorption step we have constant values of pressure, velocity, and composition which are determined by the feed gas. So, we can eliminate the integration for the adsorption step.

To calculate the specific energy consumption, we should consider different contributions:

1- Blower: To overcome the pressure drop that occurs inside the column during the adsorption step, we need to increase the pressure of the feed gas to maintain the high pressure of p_H inside the column during the whole adsorption step. To calculate this pressure drop, we can consider Ergun's equation:

$$-\frac{\partial p}{\partial z} = \frac{150}{d_p^2}\frac{(1-\varepsilon_b)^2}{\varepsilon_b^2}\mu u_{int} + \frac{1.75}{d_p}\frac{(1-\varepsilon_b)}{\varepsilon_b}\rho u_{int}|u_{int}| \tag{2.36}$$

Although we have simplified our model by neglecting the pressure drop in the column to eliminate the complexity of the model, for evaluating the specific energy consumption it is better to take this pressure drop into account. We can rewrite equation (2.36) for the whole length of the column in the adsorption step as:

$$\Delta p = \left(\frac{150}{d_p^2}\frac{(1-\varepsilon_b)^2}{\varepsilon_b^2}\mu u_{int} + \frac{1.75}{d_p}\frac{(1-\varepsilon_b)}{\varepsilon_b}\rho u_{int}|u_{int}|\right) \times L \tag{2.37}$$

The total blower work can be calculated as:

$$W_{blower}[J] = \frac{1}{\eta_{blower}}\frac{\gamma}{\gamma-1}A_{eff}p_H u_{feed}\left[\left(\frac{p_H+\Delta p}{p_H}\right)^{\frac{\gamma-1}{\gamma}} - 1\right]\Delta t_A \tag{2.38}$$

2- Vacuum pumps: In both the blowdown and evacuation steps, we should consider the work of vacuum pumps which evacuate the gas molecules from the column to maintain below-atmospheric pressure in the column. This work can be calculated as:

$$W_B[J] = \frac{1}{\eta_{pump}}\frac{\gamma}{\gamma-1}A_{eff}\int_0^{t_B} p(t)u(t)\left[\left(\frac{p_{atm}}{p(t)}\right)^{\frac{\gamma-1}{\gamma}} - 1\right]dt \tag{2.39}$$

$$W_E[J] = \frac{1}{\eta_{pump}}\frac{\gamma}{\gamma-1}A_{eff}\int_0^{t_E} p(t)u(t)\left[\left(\frac{p_{atm}}{p(t)}\right)^{\frac{\gamma-1}{\gamma}} - 1\right]dt \tag{2.40}$$

2.4. Numerical Modelling Using MATLAB

The general approach that we are following to solve model equations, begins with some assumptions and data related to sorbent characteristics, column geometry, etc.

which are given to the program as inputs. The results of solving all the model equations are the gas composition inside the column and velocity at each node alongside the column. With these computed values, we can proceed with calculating molar flows and component powers which are the prerequisites of performance indicators calculation. We can see these steps in Figure 2.5 as follows:

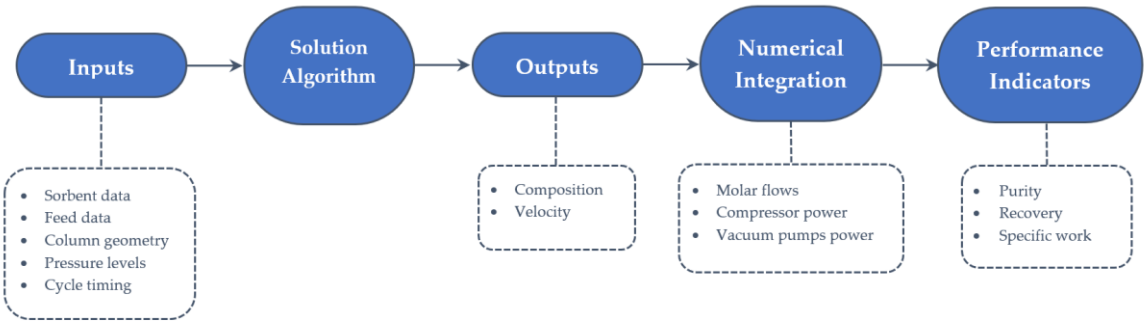

Figure 2.5: General steps that are followed in model implementation.

To implement mass balance for each process step, we start solving the system of equations (2.25) to (2.27) during each time step and update the velocity field using equation (2.28). As we are dealing with coupled stiffed DAEs in our problem, we should implement a numerical solution approach instead of solving them analytically which is not possible in this case. To do so, we developed a **MATLAB** code and implemented all the model equations. We chose the **ode15s** numerical solver due to the stiffed inherent of the DAEs that must be solved during each time step (t_K^{step}) in process step K.

After solving our equations for the first process step (K) during all its period (t_K), the final condition is read as the initial condition for the next process step. We do this process until reaching the Cyclic Steady State (CSS) in which there are no changes in the computed variables from one cycle compared to the next one. This state should be considered as the condition through which our system performs.

As we can see in Figure 2.6, reaching the CSS is the final step of the solution algorithm. In case we see a deviation in calculated variables (such as composition or velocity field) in the last cycle compared to the previous one, we should increase the number of cycles that we have initially guessed to obtain CSS. If we initially assume a very high $N_{cycle,CSS}$ value, we can make sure to reach the CSS in our first run, but at the expense of large computational time. So, we prefer starting with values around $N_{cycle,CSS} = 200$ which is a good number in our model to make sure that CSS is achieved.

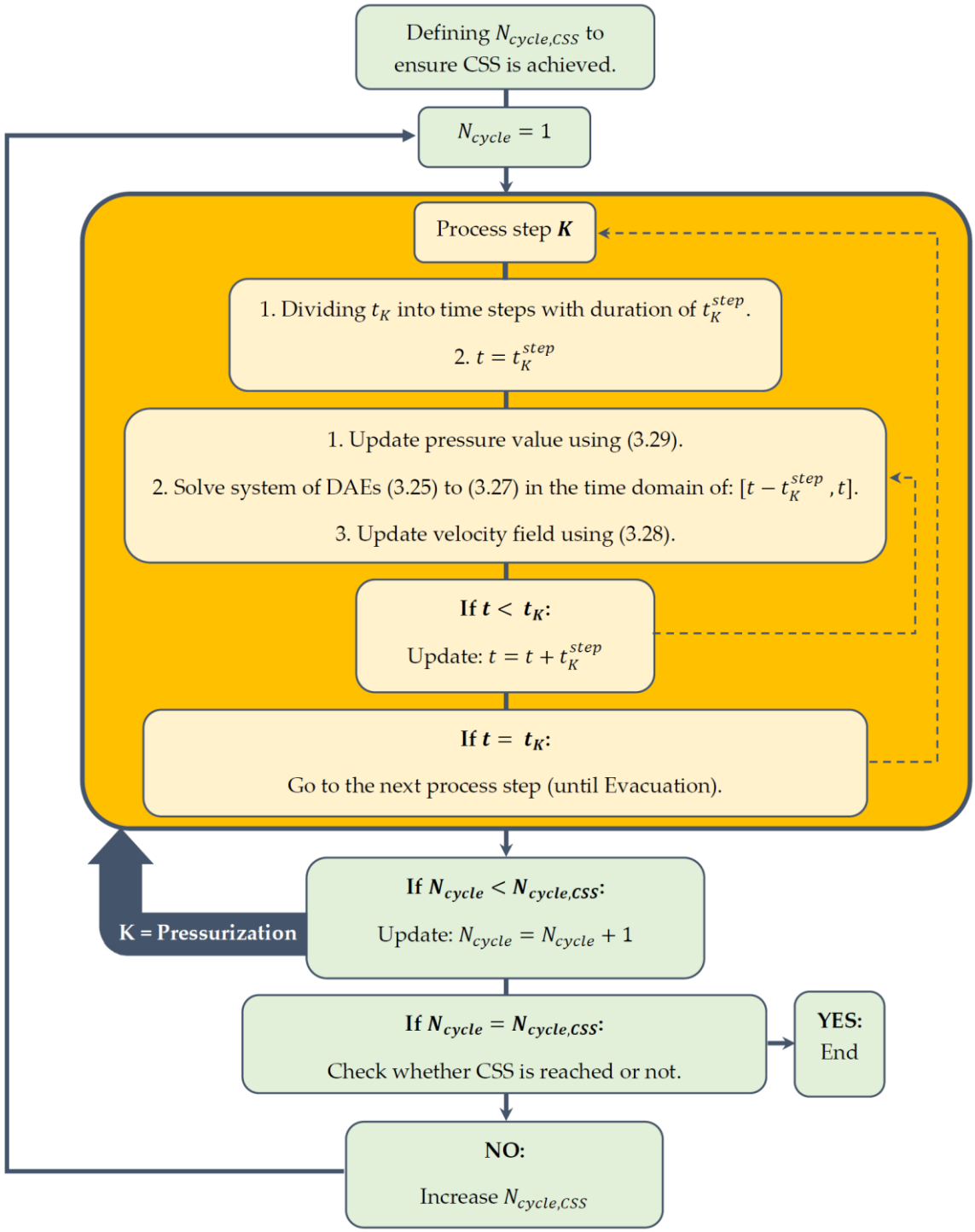

Figure 2.6: Solution algorithm implemented in MATLAB for solving model equations and reaching Cyclic Steady State (CSS).

By defining proper matrices, we can store the values of composition and velocities at the end of each process step at CSS. These data will be then executed in numerical integration procedures to calculate the number of moles (using equations (2.32)to (2.35)) entering or exiting during each process step which are the prerequisites for calculations of purity and recovery. Similarly, we can use these data for the calculation of total electrical energy that is consumed by each piece of equipment during the whole cyclic process (using equations (2.38) to (2.40)) as well as calculating average power consumption.

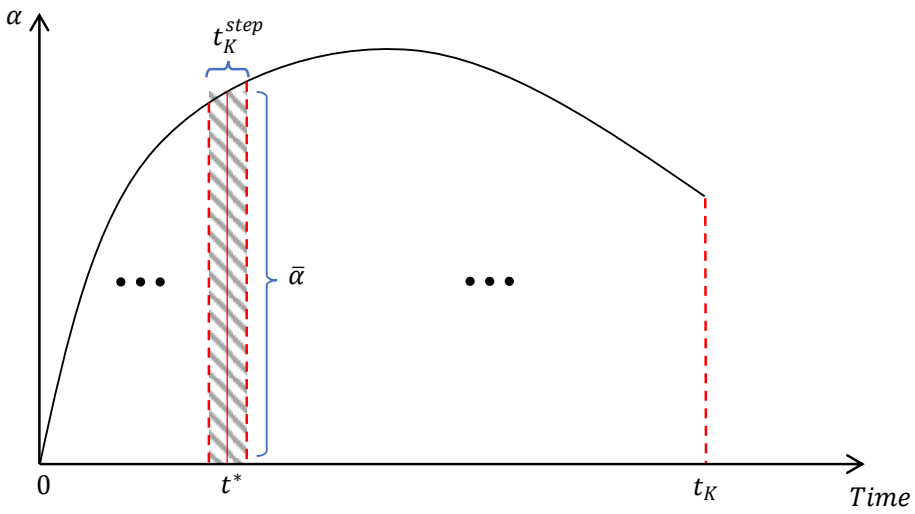

Figure 2.7: Numerical integration representation.

In Figure 2.7 we can see the numerical integration approach that we used. Considering α as a general calculated variable which varies over time, at t^*, we have considered the average variable value in the period of $\left[t^* - \frac{t_K^{step}}{2}, t^* + \frac{t_K^{step}}{2}\right]$. By dividing the whole domain into infinitesimal rectangles like the one depicted in Figure 2.7, we can calculate the whole surface below the curve which represents the integration of variable α over time.

As we can see, t_K^{step} plays an important role not only in solving the model equations but also in the accuracy of calculated integral. We can decrease the t_K^{step} to avoid over/under-estimation wherever we want to increase the accuracy of our calculation.

2.5. Model Calibration

To evaluate the level of accuracy of our model, we have validated it with the data obtained by Haghpanah et al.[4] who have developed a 4-step VSA cycle. All the data and assumptions such as sorbent characteristics used in this section are extracted from this reference to perform this validation on the same basis.

Before doing this comparison, it is worth mentioning that some simplifying assumptions that we have used in our model such as the isothermal adsorption process and neglecting pressure drop alongside the column are predicted to be the main sources of deviation compared to this reference work.

Table 2.3: Zeolite 13X data and characteristics[4].

Adsorbent name	Zeolite 13X
Adsorbent density, ρ_s $\left[\frac{kg}{m^3}\right]$	1130
Particle porosity, ε_p $[-]$	0.35
Sorbent bed porosity, ε_b $[-]$	0.37
Particle diameter, d_p $[m]$	2×10^{-3}
Molecular diffusivity, D_m $[\frac{m^2}{s}]$	1.6×10^{-5}
Tortuosity, $\tau'[-]$	3

The sorbent that is used in our work is Zeolite 13X that its characteristics are given in Table 2.3. The column is initially considered to be saturated with 100% N_2 at low-pressure level (p_L).

Table 2.4: Operating condition used in the calibration cases.

Feed gas composition	15% CO_2 85% N_2
Pre-determined feed gas velocity during the adsorption step	$u_{feed} = 1\frac{m}{s}$
Pressure levels	$p_H = 1\ bar$ $p_I = 0.2\ bar$ $p_L = 0.1\ bar$
Temperature	$T = 298K$
Steps timing	$t_P = 15s$ $t_A = 15s$ $t_B = 30s$ $t_E = 40s$
Column length	$L = 1m$

Operating conditions for this base case are reported in Table 2.4. With these operating conditions and assuming pressure profile behavior as reported in

equation (2.29), we can see the changes in pressure for one complete cycle of the process as in Figure 2.8 depicted below:

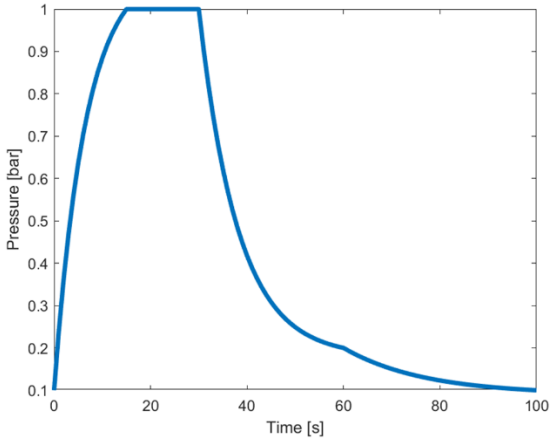

Figure 2.8: Pressure profile for calibration cases.

2.5.1. Base Case

In this base case, we have assumed mass transfer coefficients for both CO_2 and N_2 equals to 0.3 which is reported by Chue et al.[27] as a good value to fit their model to experimental data for CO_2 separation from CO_2/N_2 gas mixture using Zeolite 13X as sorbent medium. Besides, we have divided our column into $N = 100$ number of slices and solved mass balance equations for $t_K^{step} = 1s$ for each process step (K) during the step's timing reported in Table 2.4.

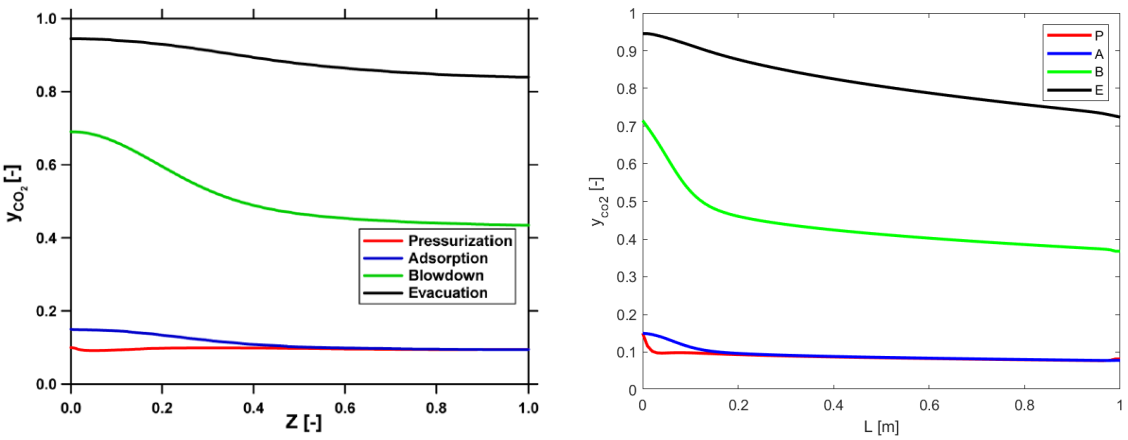

(a) (b)

Figure 2.9: Gas phase composition at CSS at the end of each step for the base case: (a) Haghpanah et al.[4] (b) This work.

Choosing $N_{cycle} = 200$ to make sure of reaching the CSS condition, the resulted gas composition alongside the column for each step is shown in Figure 2.9.

We can see in Figure 2.9, as Haghpanah et al.[4] have used the finite volume method and hence an average composition value between walls for each node, the concentration of CO_2 at the first node varies from the feed composition. However, as we have considered slice walls as column nodes, the corresponding point in our result shows the CO_2 concentration in the feed gas which is imposed as a boundary condition during the pressurization step.

Another important deviation is the length of the mass transfer zone. As we can see in Figure 2.9(a), in all the steps the changes of composition alongside the column occur with a slighter slope compared to our case's results in Figure 2.9(b). One of the main reasons is the variation of the mass transfer coefficient which plays an important role in defining the rate through which the mass transfer occurs. Another reason is the isothermal adsorption that we assumed initially in our model. In reality, during the adsorption, the heat of adsorption is released and causes the gas expansion throughout the column due to an increase in gas temperature. This leads to an increase in the CO_2 concentration alongside the column during pressurization and adsorption (similar reasoning can be said for the desorbing steps i.e. blowdown and evacuation where endothermic desorption causes a decrease of the gas temperature).

In Figure 2.10, we can see the variation of velocity during each process step. During the pressurization, we have a sudden increase in velocity as the highest pressure difference should be dealt with during this step (from p_L to p_H). As this velocity increase occurs in the initial seconds during the pressurization step, it is important to increase the resolution (increasing t_P^{step}) in which we are solving the mass balance equations and updating the velocity field. Otherwise, we are underestimating the amount of feed that enters the column during the pressurization step which ultimately results in inaccuracy in the calculation of recovery in equation (2.31).

Haghpanah et al.[4] also reported purity and recovery values of 88.74% and 35.83%, respectively. While the solutions of our model give the corresponding values as 85.60% and 50.70%. Due to the sources of deviation that we have discussed above, these variations are reasonable and we have tried to address these issues in the next section, throughout the calibrated case.

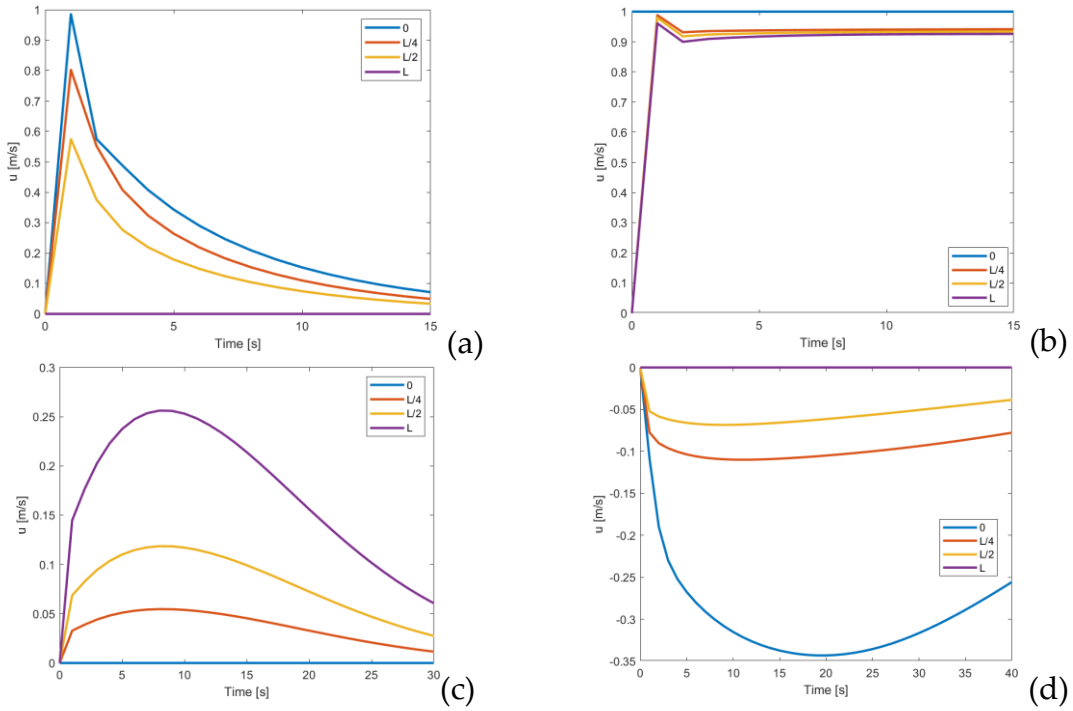

Figure 2.10: Velocity profile for the base case at CSS at different column heights during (a) Pressurization (b) Adsorption (c) Blowdown and (d) Evacuation.

As we can see from Figure 2.10(b), during the adsorption, velocity and consequently the flow rate decreases as we are moving towards the top of the column. In fact, as the CO_2 is adsorbed in a constant pressure of p_H, this decrease in velocity shows that N_2 is mainly exiting from the column product end.

By performing evacuation during the blowdown and evacuation steps, the velocity increases up to a certain point in each level alongside the column and then decreases as the pressure gradients become smaller over time. These effects can be seen in Figure 2.10(c) and (d). Note that the negative velocity during the evacuation step is due to the counter-current evacuation that is performed during this step.

2.5.2. Calibrated Case

In this section, we aim to perform some sort of sensitivity analysis to calibrate our model with the reference work. Two main sources of inaccuracy that were mentioned in the previous section, will be the subject of our discussion in this part.

Mass Transfer Coefficients

In the LDF model that we have used to model the mass transfer process, the mass transfer coefficients should be calculated using the equation (2.12) with the adsorbent data reported in Table 2.3. An important parameter is K_i which is a sort of Henry's constant that is fitted in different parts of the isotherm data in Figure 2.1.

As the slope of the isotherm curve deviates significantly by changing the partial pressure (especially in the low partial pressures where the adsorption occurs), we have divided the isotherm into 3 different sections and calculated the k_{LDF} for both components.

Table 2.5: Mass transfer coefficient analysis.

	$p_{min} - p_{max}$ $[bar]$	Δq_i^* $\left[\frac{mol}{kg_{sorbent}}\right]$	ΔC_i $\left[\frac{mol}{m^3_{voidage}}\right]$	K_i[i] $[-]$	$D_{e,i}$ $\left[\frac{m^2}{s}\right]$	$k_{LDF,i}$ $\left[\frac{1}{s}\right]$
CO_2	$0 - 0.15$	3.45	6.05	1096.1	$1.70E-09$	0.03
	$0.15 - 0.6$	0.94	18.16	100.0	$1.87E-08$	0.3
	$0.6 - 1$	0.33	16.14	39.6	$4.72E-08$	0.7
N_2	$0 - 0.15$	0.05	6.05	14.8	$1.26E-07$	1.9
	$0.15 - 0.6$	0.15	18.16	15.4	$1.21E-07$	1.8
	$0.6 - 1$	0.14	16.14	16.1	$1.16E-07$	1.7

As we can see from Table 2.5, the mass transfer coefficient is more sensitive to the pressure for CO_2 compared to the N_2. In case we want to choose an average mass transfer coefficient for both components, it must be closer to the feed composition (i.e. for low CO_2 partial pressure and high N_2 partial pressure).

On the other hand, we are considering constant temperature based on the isothermal adsorption assumption. But the temperature can affect the mass transfer coefficient due to its effect on the concentration. Dantas et al.[29] reported the overall mass transfer coefficient for Zeolite13X considering also the effect of temperature. Considering the results of our analysis in Table 2.5 and the work done by the above-mentioned authors, we chose the mass transfer coefficient of $0.15\frac{1}{s}$ for the CO_2 and $1.5\frac{1}{s}$ for N_2. So, we will proceed with the calculation of this calibrated case based on these values.

Time Step Resolutions

From Figure 2.10, we can see the sudden increase in the initial seconds of the pressurization step. We have reached the maximum velocity at $t = 1s$. This could be one of the main reasons for the recovery overestimation. In fact, as we chose the $t_P^{step} = 1s$, we only update the velocity field after the initial second of the pressurization step. Besides, we solved the mass balance equations for pressure value at $t = 1s$, during the whole first second of the pressurization step.

[i] For calculating K_i, it is important to pay attention to the units of Δq_i^* and ΔC_i. We should transform them to the same basis by considering the effect of sorbent density (ρ_s) as well as the sorbent bed porosity (ε_b).

By increasing the resolution of the pressurization time step, we have changed t_P^{step} to $0.5s$ and considering average pressure at each time step in which the model is solving the mass balance equations. By doing so, we tried to avoid underestimation of feed that enters the column during pressurization at the cost of higher computational time.

Results

By applying these modifications to our base case, we can reproduce the composition alongside the column at each process step in CSS, as depicted in Figure 2.11.

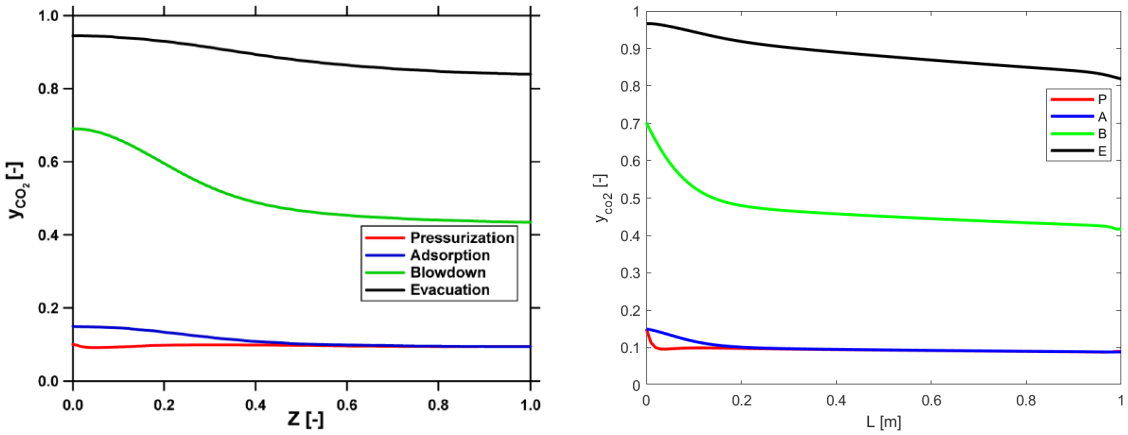

Figure 2.11: Gas phase composition at CSS at the end of each step for the calibrated case: (a) Haghpanah et al.[4] (b) This work.

Comparing Figure 2.9(b) to Figure 2.11(b), we can see that the mass transfer zone is now extended which is the result of a lower mass transfer coefficient of CO_2 that we have used for the calibrated case compared to the base one. Besides, the CO_2 composition is now closer to the value of the reference case which leads us to similar purity and recovery values. For this calibrated case the purity and recovery are calculated as 86.76.01% and 35.42%, respectively. Considering now the values reported by Haghpanah et al.[4] (88.74% of purity and 35.83% of recovery), we see that our calibrated model performance is well-enhanced.

As we have discussed in the model equations and represented in the model implementation schematic in Figure 2.5, the main outputs of our model are the gas phase composition of the gas inside the column and the velocity of the gas entering the column during the pressurization or exiting from the column during adsorption, blowdown, and evacuation steps.

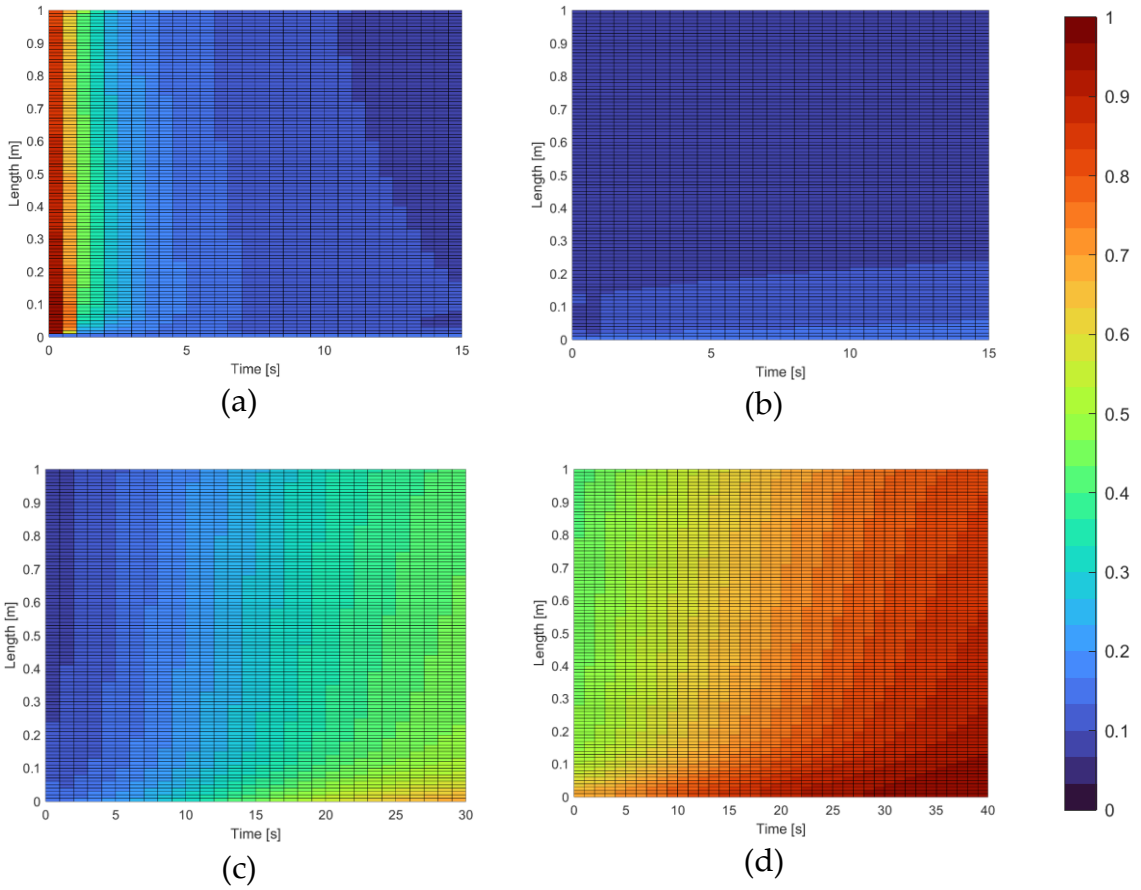

Figure 2.12: Molar fraction of CO_2 in the gas phase for the calibrated case at CSS during (a) Pressurization (b) Adsorption (c) Blowdown and (d)Evacuation.

As we can see in Figure 2.12(a), at the beginning of the pressurization step, the column is concentrated in CO_2 which is the final condition of the evacuation step. As we continuously supply feed reach in N_2, the CO_2 concentration in the column decreases until we reach the high pressure of p_H in the column. Then CO_2 is continuously adsorbed in the lower part of the column during the adsorption step.

By implementing vacuum condition at the product end of the column during blowdown, we eject the remaining amount of N_2 from the column, so the column will become rich in CO_2. As a result, during the evacuation step, we will be able to extract mainly CO_2 from the column. In Figure 2.12(d), it can be seen that during the initial seconds of the evacuation step, the outlet stream at the L=0 has still contents of N_2 ($y_{CO_2} \cong 0.65$). This will be one of the reasons that we miss purity in the evacuation step. This value increases gradually over evacuation time and at the end of this step we can capture almost 100% of CO_2.

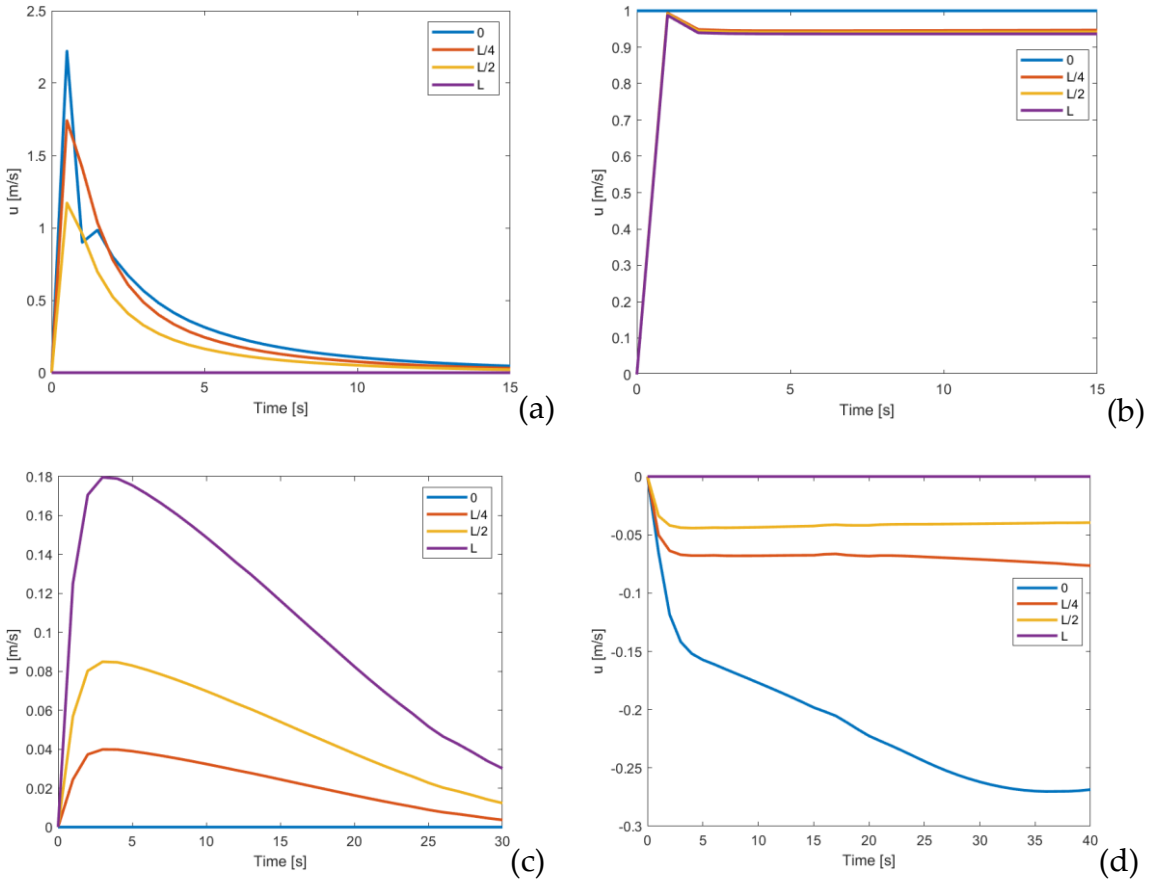

Figure 2.13: Velocity profile for the calibrated case at CSS at different column heights during (a) Pressurization (b) Adsorption (c) Blowdown and (d) Evacuation.

Due to the changes that we have implemented in the calibrated case in terms of time step resolution, comparing Figure 2.13 to Figure 2.10, we can see the calibrated model calculated higher gas velocity at the initial period of the pressurization step. Besides, as we decrease the value of the CO_2 mass transfer coefficient, CO_2 is now desorbed from the sorbent bed at a slower rate. As a result, we can see the peak velocity has been decreased for both the blowdown and evacuation steps in the calibrated case.

3 Large-scale Implementation

3.1. CO_2 Capture from WtE Plants

There are around 2100 WtE facilities all around the world which have an overall treatment capacity of 330 million metric tonnes of municipal solid wastes (MSW) per year[30]. Treatment 1 *tonne* of MSW in the WtE plant results in 0.7 *tonnes* of CO_2 emission. In Figure 3.1, we can see that around 1% of the global CO_2 emission comes from WtE plants.

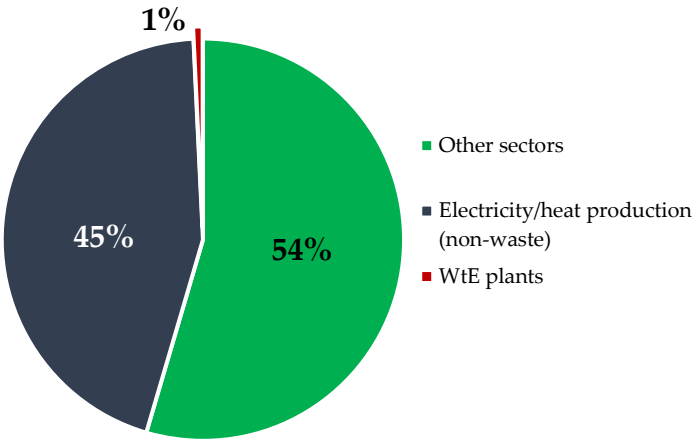

Figure 3.1: Global CO_2 emission.

Around half of this CO_2 has biogenic roots that resulted from the combustion of carbon content in the MSW with biological roots. This portion can be considered as natural CO_2 circulation in nature and hence, carbon neutral. Although this biogenic fraction highly depends on the composition of MSW treated in the WtE facility, in general, we can say that CO_2 capture from the WtE plants results in a net negative CO_2 emission and make this sector an interesting option for decarbonizing the energy sector.

One of the main issues that resist the development of the CO_2 capture systems is the high energy penalty that they impose on the host plant. This is even more crucial in WtE plants due to the higher cost of final energy production due to special facilities required in such plants to recover the thermal energy of wastes. Another issue is the dynamic operation of most WtE facilities providing both heat and electricity in the

summer or winter. Adding solvent-based CO_2 capture requires heat integration strategies that impose further complexity on the operation of such plants.

Implementing VSA to WtE plants can diminish these complexities and avoid the decrease in the efficiency of the whole plant thanks to the lower energy consumption. In addition, a CO_2 negative WtE plant is socially more attractive and avoids public objections about such plants. The captured CO_2 can be further utilized for fossil-free fuels such as methanol which provides an additional revenue stream for the plant's owner.

Currently, there are a handful of projects worldwide related to CO_2 capture integration to WtE plants. They are capable of partial recovery of CO_2 from the plant and either store or utilize the captured CO_2. All of these facilities are implemented solvent-based post-combustion CO_2 capture systems at expense of a high thermal energy penalty they impose on the host plant. In Table 3.1, we can see plenty of these facilities and the capacity of MSW treated yearly.

Table 3.1: Number of recognized WtE facilities with CCS implementation projects.

Plant	Country	Capacity $\left[\frac{tonne_{MSW}}{year}\right]$	Status	Ref.
Fortum Oslo Varme	Norway	400′000	-Pilot (1:350 scale): Testing campaign.	[31]
Twence-Hengelo	Netherlands	600′000	-Pilot (1:50 scale): Under operation. -Full scale: Contract signed on 2019.	[32]
Amager Bakke	Denmark	600′000	-Full scale: Feasibility study.	[33]
Vatenfall Uppsala	Sweden	200′000	-Full scale: Feasibility study.	[34]

3.2. WtE Plant Data of The Case Study

The Waste-to-Energy plant of our case study takes 70 $\frac{tonne_{MSW}}{hour}$ which is treated in 3 identical lines (Equal to around 550′000 $\frac{tonne_{MSW}}{year}$). This MSW flow rate corresponds to 220 MW_{th} of thermal energy supplied to the plant to provide steam at 425℃ and 50 bar. Finally, the plant generates 64 MW_{el} of electrical power through 3-stage steam turbines in its summer mode in which no heat is supplied to the district heating network.

In this work, we aim at proposing a Carbon Capture system to capture CO_2 from this plant's flue gas that its characteristics are reported in Table 3.2 as below:

Table 3.2: WtE plant flue gas characteristics.

Composition	[%***mol***]
CO_2	10.06%
N_2	69.57%
O_2	6.00%
H_2O	14.37%
Total molar flow rate	4.34 $kmol/s$
Number of trains	3
Temperature	135℃
Pressure	1 bar

3.3. Large-Scale Design Methodology

3.3.1. Design Target

Referring to Figure 2.4, 4 separate steps should be done to separate CO_2 from the feed gas in the VSA process. Every step can start only after its predecessor process step is done. Hence, with just one column, the VSA process is inherently a batch process rather than a continuous process.

However, by increasing the number of columns and proper process timing, we can supply continuous feed to the VSA system which makes it a continuous capture process.

Continuous Feed Supply

To have a continuous VSA process, we need to supply the feed gas continuously supplied in the adsorption step. It means that at least we need 2 separate columns. So, when the first column is in the adsorption mode, the second column's bed is regenerated and pressurized to be ready for the adsorption step.

The adsorption step is the only step in which we can define the rate of the feed that is supplied to the column. The gas velocity entering or exiting the pressure-varying steps is continuously changing. Hence, we cannot even combine pressurization and adsorption steps if we want to supply continuous feed to our system.

By supplying the whole flue gas during the adsorption step with a specified rate, we cannot supply the gas required for pressurizing the column. To address this issue, we can follow two different approaches:

1- Pressurization with a fraction of flue gas: In this scenario, prior to using the flue gas for the adsorption, we must extract a partial amount of feed to be used during the pressurization. Hence, this fraction is used at the intervals we need pressurization occurs in one of the columns. The amount of this flue gas fraction

should be calculated based on some designed variables such as pressurization and adsorption timing and the predefined interstitial feed velocity during the adsorption step.

However, unlike the feed used in the adsorption step, this fraction is not continuously used in the whole cycle duration due to the shorter pressurization duration compared to the adsorption. Besides, we can not further supply it to the column during the adsorption step as this step performs at a constant rate. Hence, we should emit this fraction into the atmosphere when there is no need for pressurization in non of the columns. As we can see, this option penalizes the total recovery of the process significantly.

2- Pressurization with the light product: An effective alternative to the previous approach is to supply the gas needed for the pressurization step, with the product gas that exits the column during the adsorption step. This gas mainly consists of N_2 as the CO_2 is preferentially adsorbed during this step. So, we can pressurize a column with the product gas of another column that is operating in the adsorption mode as depicted in Figure 3.2. With this approach, we can make sure that pressurization is performed completely, without penalizing the recovery of the plant.

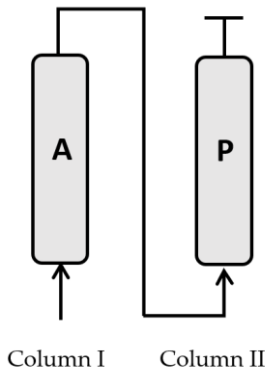

Figure 3.2: Pressurization with the light product.

Pressurization with the light product is also discussed by Krishnamurthy et al.[24] and tested in their pilot set-up referring as Light Product Pressurization (LPP) as it mainly consists of N_2 which is the light component in the product stream. As they discussed, by implementing LPP, the CO_2 that is not adsorbed during the adsorption step can be further recovered by recycling the product gas to pressurize the system. For a target purity of 95%, they achieved an almost 15% increase in the recovery in the case of implementing LPP compared to the basic 4-step VSA process.

Cycle Timing

As we discussed in the previous part, a 2-column system requires a minimum number of columns in which we can have a continuous capture process. However, in the case of implementing VSA for capturing CO_2 from flue gas, it negatively affects the level of purity and recovery that we can obtain from our system. The main reason is that the longest process period is generally dedicated to the evacuation step in which we recover CO_2 that is previously adsorbed in the column. According to several works that study a similar configuration[4,24], the evacuation period is 2-5 times higher than the adsorption period for achieving purity and recovery levels higher than 90%.

A more accurate approach is conducting a full optimization problem with all the process variables (such as process timings, pressure levels, and feed gas velocity) to maximize purity and recovery. However, based on the above-mentioned results in the literature, the lowest possible footprint of the adsorption process while maintaining a continuous feed and relatively high purity and recovery levels (around 90% in an optimized scenario), is a 4-column system.

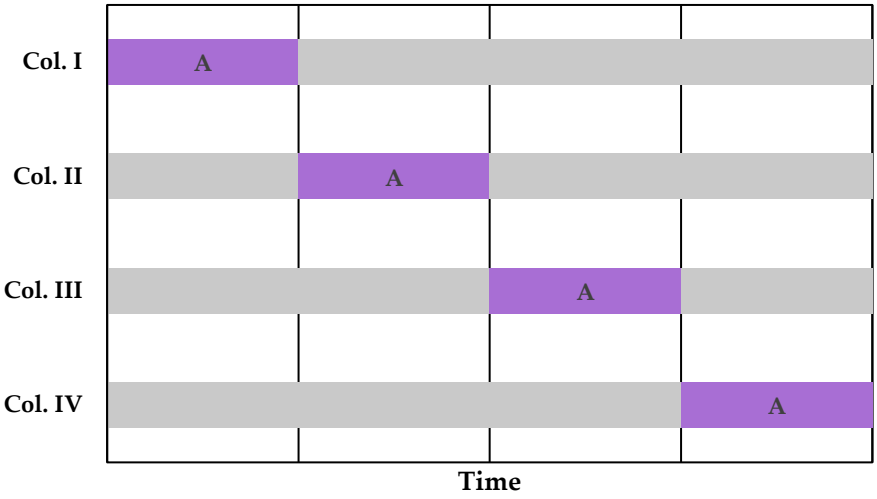

Figure 3.3: Continuous VSA process timing scheme with 4 columns.

In Figure 3.3, we can see the schematic of the process timing considering the feed is continuously supplied to the system. In this 4-column scenario, the time available for the pressurization, blowdown, and evacuation steps combined (the gray area) is 3 times the adsorption period (the purple area).

It is important to recall that this 4-column process is proposed to provide enough evacuation period while minimizing the footprint of the whole VSA plant which is reported to be very high in the case of retrofitting large-scale plants with CO_2 capture through pressure swing adsorption.[3]

Another important point we can notice is that when one column is in the adsorption mode, the other three columns are working in either the blowdown or the evacuation (excluding pressurization which is relatively short). This means that 3 vacuum pumps should work simultaneously in order to maintain this continuous VSA process. This is crucial in either calculating the total specific energy consumption and cost estimation.

3.3.2. Column Sizing

To design the geometry of the columns, first, we should consider the total flue gas characteristics that we want to be treated in the VSA system which is reported in Table 3.2. As we discussed in the previous chapter, due to the hydrophilic characteristics of Zeolite 13X, we must dry the flue gas before supplying it to the adsorption column. In the drying process, we assumed that all the water content is removed from the flue gas and its temperature is reduced to 25℃.

Besides, to simplify the simulation process we can assume the dried flue gas as a binary mixture of CO_2 and N_2. This is relatively an acceptable assumption as the N_2 and O_2 behave almost similar in contact with Zeolite 13X in terms of selectivity and saturation capacity.[3,5] As we can see in Figure 3.4, by implementing these assumptions, the flue gas that finally enters the VSA plant is assumed to consist of $12\%_{vol}$ of CO_2 and $88\%_{vol}$ of N_2.

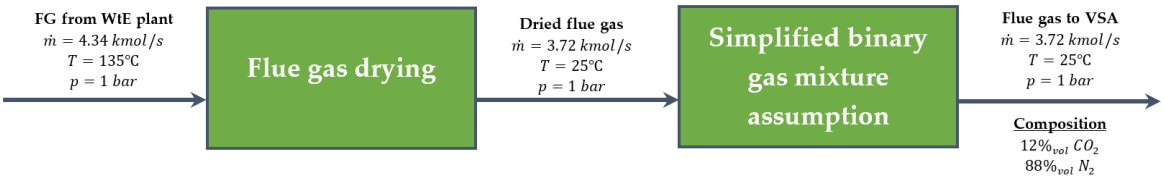

Figure 3.4: Flue gas conditioning before entering the VSA plant.

As the reference plant is treating MSW in 3 identical lines, we are targeting designing the VSA plant for a single line. So, the whole VSA plant consists of 3 identical VSA systems as well. The flue gas volumetric flow rate entering each VSA system considering ideal gas law can be calculated as:

$$\dot{V}_{FG,per\ WtE\ train} = \frac{\dot{V}_{FG,total}}{3} \tag{3.1}$$

$$\dot{V}_{FG,per\ WtE\ train} = \frac{1}{3}\left(3.72\frac{kmol}{s} \times 8.314\frac{kJ}{kmol.K} \times 298.15K\right)$$

$$\dot{V}_{FG,per\ WtE\ train} = 30.72\frac{m^3}{s}$$

As we discussed in the previous part, our main limiting design consideration is the minimum achievable footprint. For this purpose, we want to handle as much feed gas to be handled in one single column during the adsorption as possible. Two main constraints for reaching this purpose are related to the pressure drop alongside the column during the adsorption step. Firstly, according to the Gas Processors Supplier Association (GPSA) the maximum pressure gradient of $7.5\frac{kPa}{m}$ is allowable during the adsorption step.[35] So considering Ergun's equation for the pressure drop (equation (2.36)), Zeolite 13X characteristics reported in Table 2.3, flue gas viscosity of $1.72E-5\frac{kg}{m.s}$ and mass density value of $1.2\frac{kg}{m^3}$, we can calculate the maximum allowable interstitial gas velocity:

$$u_{feed}^{max} = 1.59\frac{m}{s}$$

Secondly, GPSA suggests a maximum total pressure drop of $55\,kPa$ in the adsorption column.[35] In this work, we considered a more cautious value of 52 kPa. Using Ergun's equation, this value gives us the maximum allowable column height as:

$$L_{column}^{max} = 7.0\ m$$

Subreaveti et al.[5] suggest the length-to-diameter ratio of the column be between 2 and 6. This value is suggested based on commonly used adsorption columns working in large-scale industries. Hence, we can calculate the maximum allowable column diameter as:

$$D_{column}^{max} = \frac{L_{column}^{max}}{2} \tag{3.2}$$

$$D_{column}^{max} = 3.5\ m$$

Now, we can proceed with calculating the maximum gas flow rate that the column can take as input. First, we should calculate the maximum allowable column cross-sectional area as:

$$A_{column}^{max} = \pi\frac{{D_{column}^{max}}^2}{4} \tag{3.3}$$

$$A_{column}^{max} = 9.6\ m^2$$

The effective cross-sectional area of the column in which gas can move with its interstitial velocity should be decreased by ε_b parameter as we discussed in equation (2.6a). So, we can write:

$$A_{eff}^{max} = A_{column}^{max} \times \varepsilon_b \tag{3.4}$$

$$A_{eff}^{max} = 3.6\ m^2$$

Now we can calculate the maximum flue gas volumetric flow rate that can be handled in one column:

$$\dot{V}_{per\ column}^{max} = A_{eff}^{max} \times u_{feed}^{max} \tag{3.5}$$

$$\dot{V}_{per\ column}^{max} = 5.7 \frac{m^3}{s}$$

Now, we can calculate the minimum number of VSA trains needed to handle the flue gas from each WtE plant's line:

$$\#VSA\ trains_{per\ WtE\ line}^{min} = \frac{\dot{V}_{FG,per\ WtE\ train}}{\dot{V}_{per\ column}^{max}} \tag{3.6}$$

$$\#VSA\ trains_{per\ WtE\ line}^{min} = 5.4$$

As we must have integer numbers of VSA trains, rounding up the calculated value to the nearest higher integer value gives us the total train number of 6. Then, we can calculate the real column dimensions by targeting this number of VSA trains per WtE line recalculating the previous steps. In Table 3.3 we can see the final results:

Table 3.3: Summary results of the column geometry calculations.

$\boldsymbol{L_{column}}$	$6.7\ m$
$\boldsymbol{(L/D)_{column}}$	2
$\boldsymbol{D_{column}}$	$3.3\ m$
$\boldsymbol{u_{feed}}$	$1.59\ m/s$
$\boldsymbol{\dot{V}_{per\ column}}$	$5.1\ m^3/s$
$\boldsymbol{\#VSA\ trains_{per\ WtE\ train}}$	6

In Figure 3.5, we can see the flowsheet of the VSA system designed for each WtE plant's line. As we can see, the flue gas is conditioned and compressed to the state suitable for the VSA system. Then, it is divided into 6 separate VSA trains each of which we have 4 separate columns maintaining the continuous feed and 3 vacuum pumps that work simultaneously.

The product stream of the adsorption step is used for the pressurization of the successor column when it is necessary. Otherwise, it vents out into the atmosphere. The exiting stream of the blowdown step mainly consists of N_2 and is directly

released into the atmosphere, while the evacuation exiting stream is directed into either CO_2 compression or purification unit to become suitable for storage.

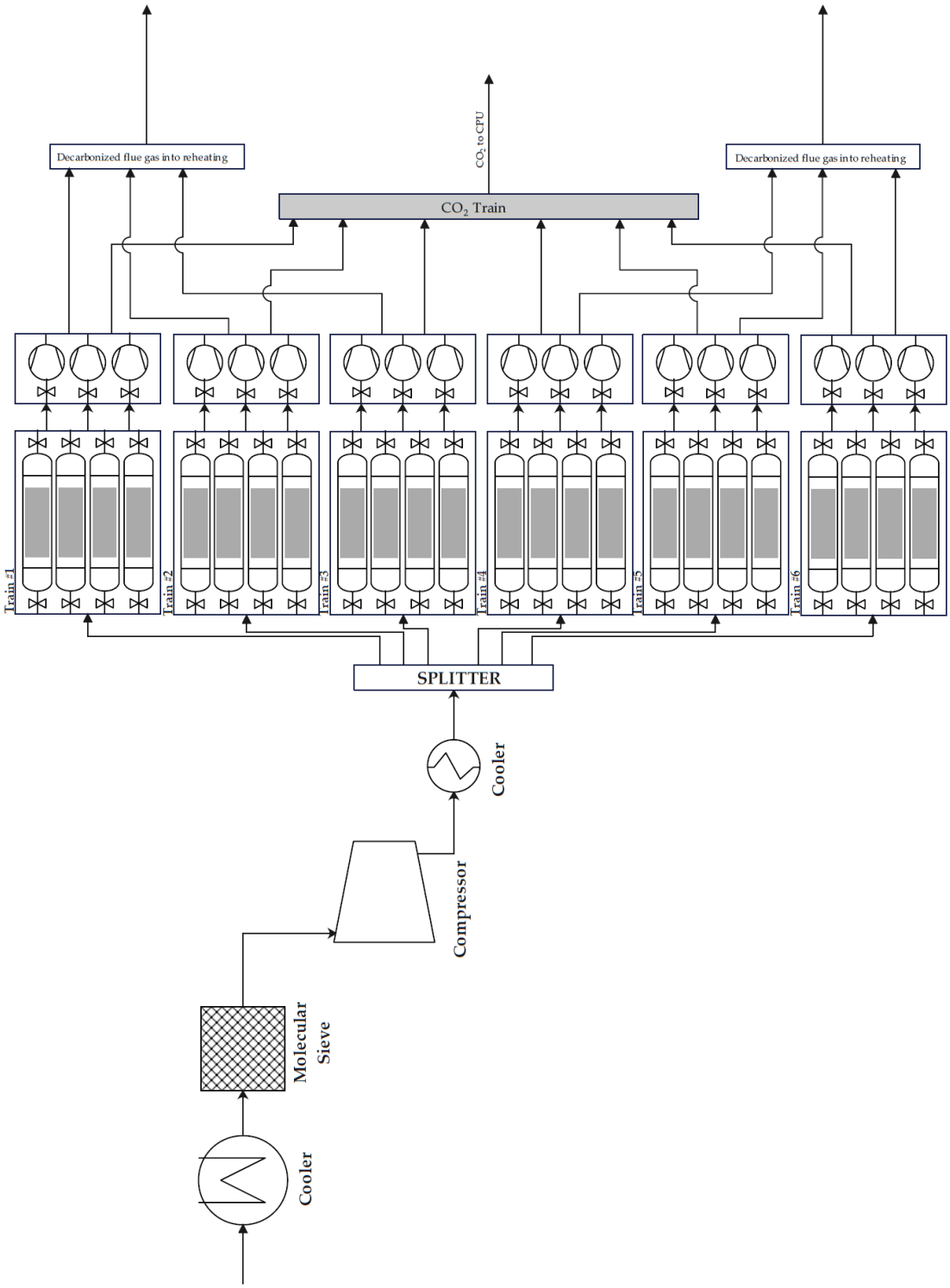

Figure 3.5: Flowsheet of a 6-train 4-column VSA system designed for each WtE line.

4 Techno-Economic Assessment

4.1. Base Case

4.1.1. Operational Data and Assumptions

To define a base case for modeling the process, we need to assume values for the main operating parameters namely the operating pressures (p_H, p_I, p_L) and step timing required for each process step to be completed (t_P, t_A, t_B, t_E). Another main operating parameter is the feed velocity which we have calculated in the previous part by assuming the largest possible volume flow rate of gas that can be handled in one single column.

As we are performing adsorption at almost atmospheric pressure, hence we have $p_H = 1\ bar$. For choosing the values for the other 6 operating parameters that can maintain acceptable purity and recovery range, we reviewed a couple of works that have analyzed similar 4-step VSA cycles as our case.[4,5,24] In all the cases, they have reported p_I values between 0.1 and 0.3 bar and p_L values between 0.01 and 0.03 bar for reaching purity and recovery higher than 90%. Hence, in the base case, we have assumed p_I and p_L values of 0.1 bar and 0.02 bar, respectively.

As previously discussed and depicted in Figure 3.3, we targeted a 4-column design for the full-scale plant which can maintain continuous feed with a relatively low footprint. By this assumption, we have already put a constraint for process step timing as:

$$t_P + t_A + t_B + t_E = 4t_A \tag{4.1}$$

For the base case, we assumed $t_A = 200s$ which is in line with the values suggested by Haghpanah et al.[4] for the same VSA configuration and by Subraveti et al.[5] who analyzed the same VSA configuration for a large-scale steam methane reforming plant.

As the pressurization step can be done in a relatively short period, we assumed the value of $t_P = 50s$ for the pressurization in which the required feed is supplied from the product gas of the relatively longer adsorption step. In the blowdown step, we

aim at ejecting the remaining N_2 in the column form the adsorption step. So, almost no CO_2 desorption is targeted to occur during this step. Hence, we can consider a relatively shorter time compared to the evacuation step. As an initial value, we can assume the $t_E/t_B = 5$ and allocate the remaining time from equation (4.1) for these steps. The results would be $t_B = 92s$ and $t_E = 458s$. In Figure 4.1, we can see the allocated step timings for each column to maintain the continuous feed.

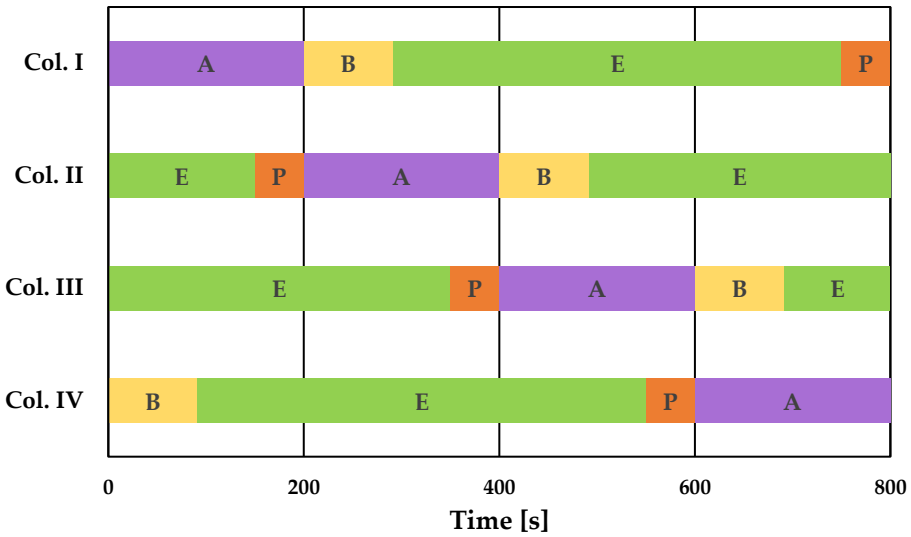

Figure 4.1: Process steps timing for the base case.

Table 4.1: Data and assumptions for the full-scale base case.

Zeolite 13X data	Table 2.3
Flue gas properties	$\rho_g = 1.2\ kg/m^3$ $\mu_g = 1.72E-5\ kg/m/s$
Mass transfer coefficients	$k_{LDF,CO2} = 0.15\ 1/s$ $k_{LDF,N2} = 1.5\ 1/s$
Pressure levels	$p_H = 1\ bar$ $p_I = 0.1\ bar$ $p_L = 0.02\ bar$
Step timing	$t_P = 50s$ $t_A = 200s$ $t_B = 92s$ $t_E = 458s$
Efficiencies	$\eta_{compressor} = 72\%$ $\eta_{vacuum\ pump} = 72\%$
Number of slices	50
$N_{cycle,CSS}$	150

We have divided the column into 50 slices in which the balance equations should be solved. A higher number of slices results in a very large computational time with a marginal effect on the outputs of our model. Besides, we have chose $N_{cycle,CSS} = 150$ to ensure that CSS is reached. All the data and assumptions given to the model as inputs for our base case are summarized in Table 4.1 as below:

4.1.2. Results

Prior to extracting performance indicators from the model results, we should make sure that CSS is reached. As we can see in Figure 4.2, after around 100 cycles, there are almost no changes in the values of purity and recovery for a cycle run, compared to the previous one. Hence, we can be confident that after 150 cycles which we have initially assumed, CSS is achieved at the end of the run.

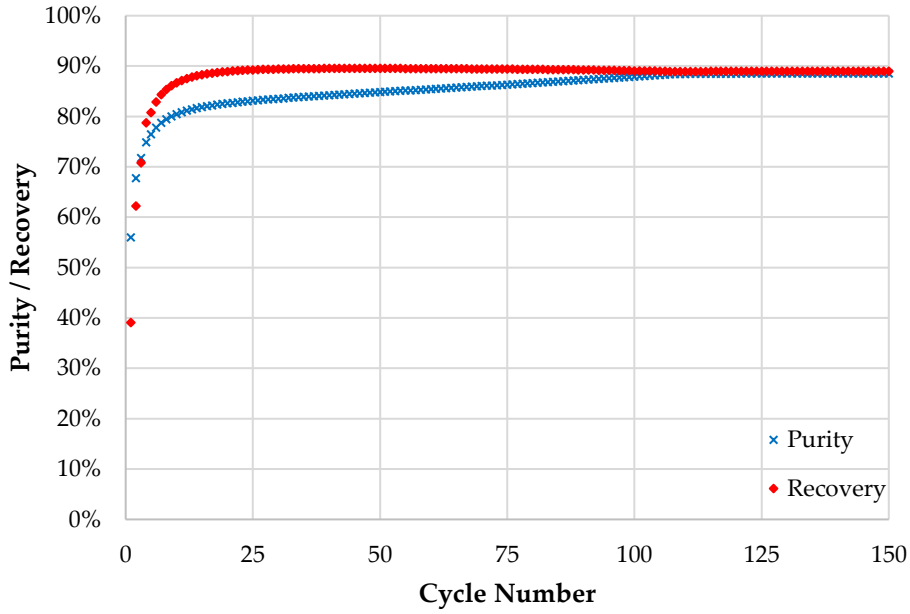

Figure 4.2: Purity and recovery for each cycle run until reaching cyclic steady state (CSS).

The values reported in Table 4.2 are the results we obtained by implementing the model for a single column. So, to calculate the overall performance of one full cycle in each VSA train, we must consider the simultaneous operation of columns during the whole cycle period. (see Figure 4.1)

Table 4.2: Performance results of the full-scale base case.

Purity	88.51%
Recovery	88.91%
Compressor power	304.1 kW_e
Blowdown power	105.4 kW_e
Evacuation power	188.9 kW_e
Specific energy consumption	225.3 $kWh_e/t_{CO_2,captured}$

The specific energy consumption would be the same as it is normalized by the amount of CO_2 captured. To calculate the total power consumption in each VSA train, we must consider the average power that is consumed during blowdown and evacuation. The blowdown and evacuation pumps are not working at each moment during the whole cycle period. So, we can calculate the average power by evaluating the total energy consumed by each vacuum pump during the whole cycle period:

$$\bar{P}_K = \frac{\#columns \times P_K \times t_K}{t_{cycle}} \tag{4.2}$$

Where K is the process step in which the power is consumed. As the compressor is working continuously to provide continuous feed to our system, we can consider its power in calculating the total power:

$$P_{total\ per\ VSA\ train} = P_{Compressor} + \bar{P}_{Blowdown} + \bar{P}_{Evacuation} \tag{4.3}$$

$$P_{total\ per\ VSA\ train} = 785.2\ kW$$

To calculate the overall power for the whole plant, we must consider the total number of VSA trains as well as all the WtE plant lines:

$$P_{VSA,overall} = \#WtE\ lines \times \#VSA\ trains \times P_{total\ per\ VSA\ train} \tag{4.4}$$

$$P_{VSA\ overall} = 14.1\ MW_e$$

4.2. Parametric Analysis

Proposing a VSA cycle that enables us to reach certain levels of purity and recovery (such as 90% of recovery and 95% of purity suggested by US-DOE), requires a complete optimization scheme in which, we should simultaneously include all the 7 operational parameters as the optimization variables to maximize the recovery and purity which is beyond the scope of this work.

However, a sort of sensitivity analysis is performed in this part to evaluate the most important operating parameters with essential effects on process performance such as purity, recovery, and energy consumption. The main aim is to propose other alternatives to our base case in which the purity or recovery level is enhanced.

4.2.1. Pressure Levels

Pressure levels are the main operating parameters of a pressure swing adsorption system as they directly affect the saturation capacity of the sorbent. Generally, at higher pressure levels, the sorbent can adsorb higher CO_2 for a certain concentration (see Figure 2.2). On the other hand, this is also important during bed regeneration where less CO_2 is desorbed from the bed if the intermediate and low-pressure levels are relatively high.

As we are dealing with a VSA cycle, the high-pressure level is assumed to be constant at $p_H = 1\ bar$ in all the cases. In Figure 4.3, we can see that by increasing p_L, as lower CO_2 is desorbed form the column, the capacity of the sorbent to adsorb CO_2 during the adsorption step will be decreased. As a result, more CO_2 is going out from the column together with N_2 during the adsorption step and we lose recovery. Increase of p_L also results in lower N_2 to be exited from the column during the evacuation step and hence the purity is increased.

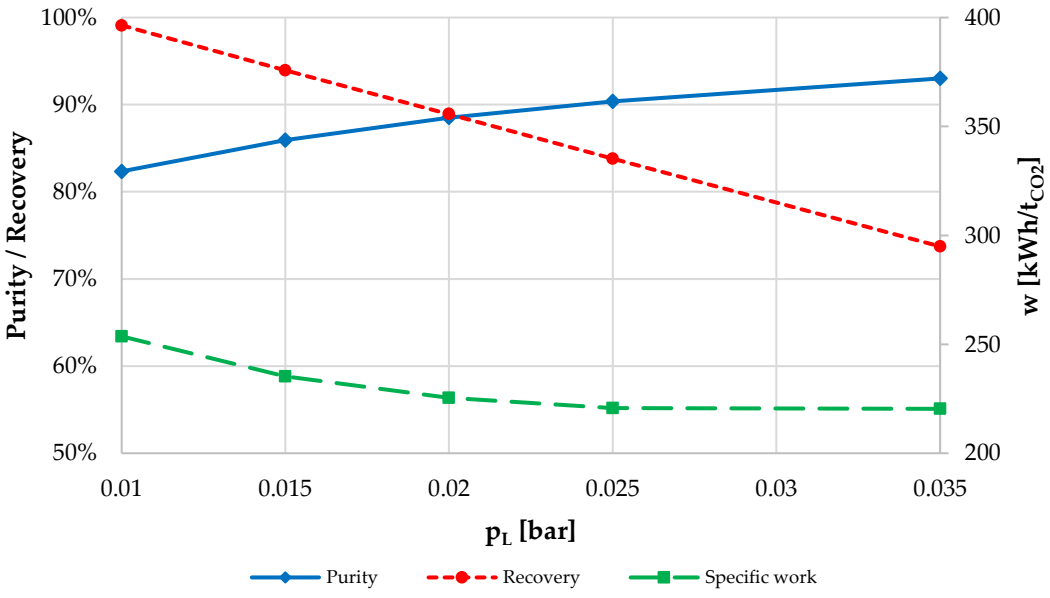

Figure 4.3: Sensitivity of performance indicators to low-pressure level (p_L).

Although the vacuum pumps total work decreased by incorporating higher p_L, the steep decrease in the recovery results in almost no changes in the specific work for the high levels of p_L until 0.035 bar. To better discuss this, we can see the different

process steps share of the total specific work in Figure 4.4. The significant effect of low recovery in the compression work can be observed. Total compression work remains the same as it only depends on the adsorption pressure which is always performing at $p_H = 1\ bar$. However, the compression specific work increases by decreasing the recovery and compensates for the decrease of both blowdown and evacuation works. Hence, the total specific work remains unchanged at high p_L.

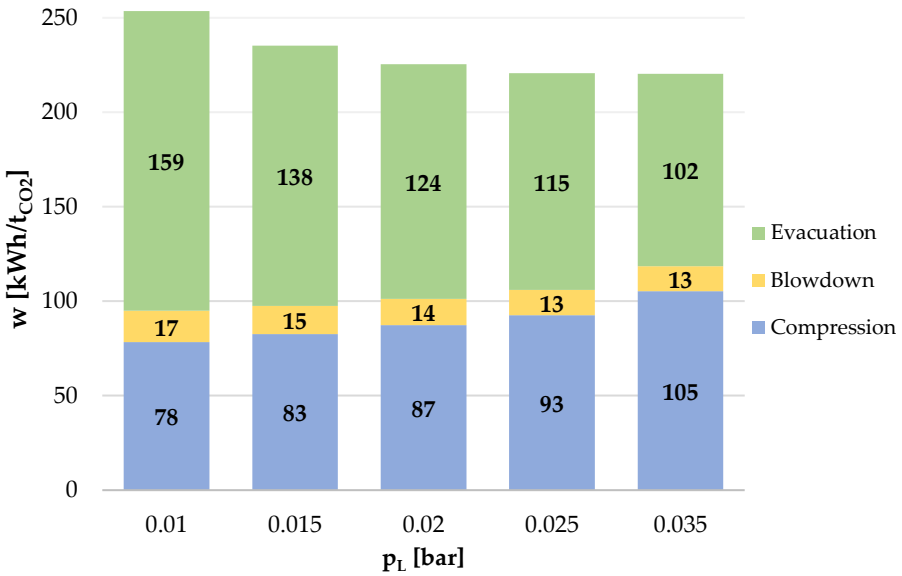

Figure 4.4: Specific work of each step for different low-pressure levels (p_L).

On the other hand, increasing the p_I has the opposite effect on purity and recovery which is shown in Figure 4.5. The main reason is that less CO_2 is desorbed and removed from the column during the blowdown step. However, as the blowdown step is relatively short, this effect is not very significant for high p_I levels. Increase in p_I adversely affect the purity as the N_2 which is not removed from the blowdown step due to high p_I is exiting with CO_2 during the evacuation step and causes a decrease in purity.

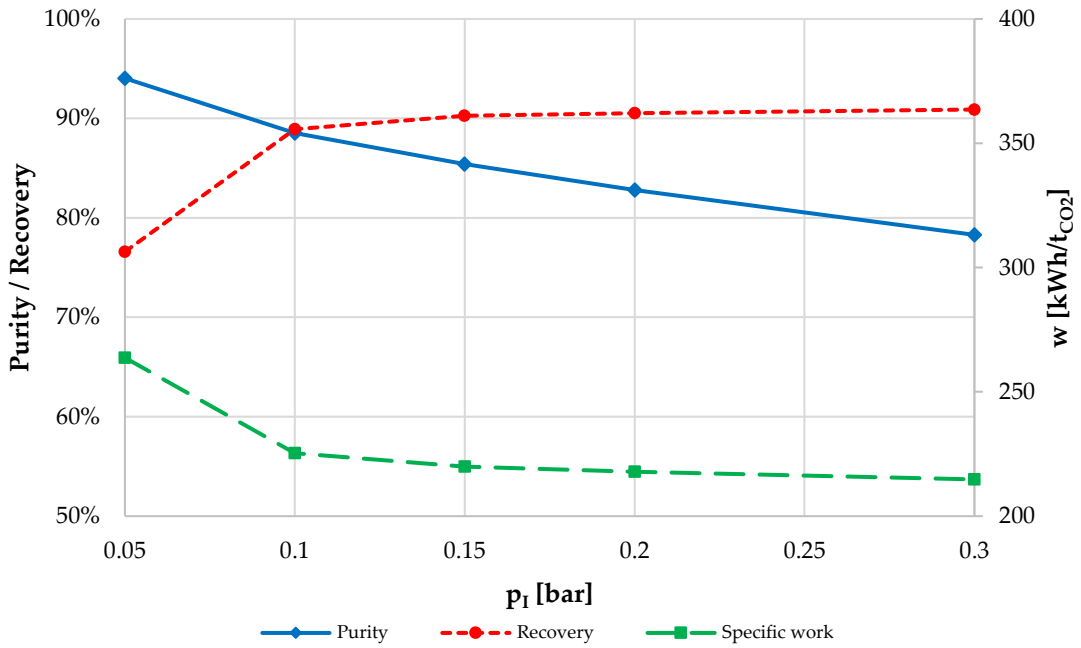

Figure 4.5: Sensitivity of performance indicators to intermediate pressure level (p_I).

The specific work behavior in Figure 4.5 is based on the fact that vacuum pump work is increasing significantly for very low vacuum levels (see equations (2.39) and (2.40)) compared to the higher ones. So, for high p_I, the decrease in the vacuum pump work is compensated by increase recovery value and the changes in specific work would not be significant.

4.2.2. Step Timing

By increasing adsorption step timing while not changing other operational variables from the base case, we can reach a higher purity level at the expense of lower recovery as we can see in Figure 4.6. An increase in adsorption duration results in longer blowdown and evacuation duration based on the scheme we proposed in Figure 3.3. Higher adsorption duration increases the fraction of the bed that is saturated with CO_2 and more general, the mass transfer area evolves to the top end of the column. So, together with a higher evacuation duration, we can extract a higher purity stream in the evacuation step from the bottom end of the column.

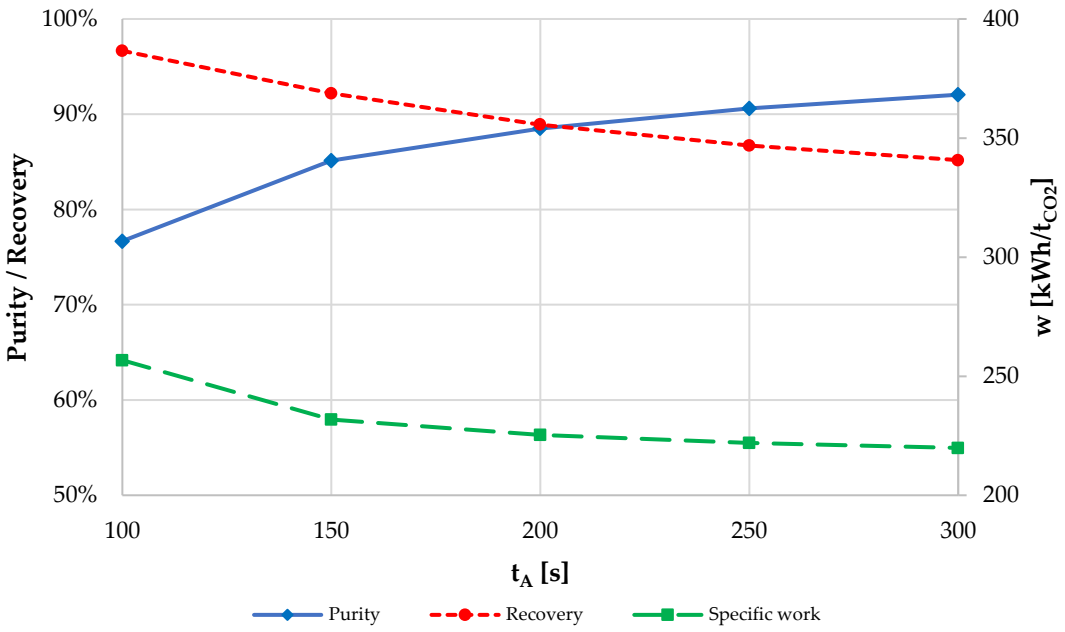

Figure 4.6: Sensitivity of performance indicators to adsorption step timing (t_A).

On the other hand, as the mass transfer zone evolves to the top side of the column, we lose more CO_2 during the adsorption step which decreases the recovery. The net effect of the increase in the adsorption duration is a decrease in the specific work as more feed is entering the column in the whole cycle, while there are no changes in the pressure levels compared to the base case.

4.3. Selected Cases with Enhanced Purity/Recovery

Based on the figures we have discussed in the previous part, reaching a high recovery requires a higher difference between p_I and p_L, meaning that we should increase the intermediate pressure and decrease the low-pressure level. This not only avoids CO_2 to exit from the column during the blowdown step, but to better regenerate the sorbent bed during the evacuation step.

On the other hand, as the difference between these pressure levels decreases, higher CO_2 and N_2 exits from the column in the blowdown step and the recovery decreases, while we have a more pure stream in the evacuation outlet stream in terms of CO_2 concentration. To summarize, each of the purity and recovery levels will enhance in terms of penalizing the other one.

In this section, we aimed at proposing two alternatives to our base case: one with a higher purity level (**Case P**) and the other one with an enhanced recovery level (**Case R**). The aim is to compare all three cases in terms of specific energy

consumption and cost of CO_2 captured which will be addressed in the economic assessment section.

Table 4.3: Operating parameters of three selected cases.

Operating Parameter	Base Case	Case P	Case R
Pressure levels	$p_H = 1\ bar$ $p_I = 0.10\ bar$ $p_L = 0.02\ bar$	$p_H = 1\ bar$ $p_I = 0.11\ bar$ $p_L = 0.016\ bar$	$p_H = 1\ bar$ $p_I = 0.08\ bar$ $p_L = 0.035\ bar$
Step timing	$t_P = 50s$ $t_A = 200s$ $t_B = 92s$ $t_E = 458s$	$t_P = 50s$ $t_A = 150s$ $t_B = 67s$ $t_E = 333s$	$t_P = 50s$ $t_A = 300s$ $t_B = 142s$ $t_E = 708s$

As represented in Table 4.3, we have selected p_I and p_L with small difference to reach the high purity and with a large difference to achieve a high recovery scenario. A longer adsorption period is selected for Case R as it promotes higher recovery (see Figure 4.6). It is worth mentioning that the initial approach that we have followed for continuous feed in a 4-column scheme is valid for all the cases. Other process parameters are the same for all three cases which are reported in Table 4.1.

The performance results are reported in Table 4.4 as below.

Table 4.4: Performance results of the three selected cases.

Performance Indicator	Base Case	Case P	Case R
Purity [%]	88.51	94.95	81.30
Recovery [%]	88.91	73.89	97.00
Compressor power $[\boldsymbol{kW_e}]$	304.1	304.1	304.1
Blowdown power $[\boldsymbol{kW_e}]$	105.4	64.7	163.3
Evacuation power $[\boldsymbol{kW_e}]$	188.9	130.3	241.5
Specific energy consumption $\left[\frac{kWh_e}{t_{CO_2,captured}}\right]$	225.3	221.7	240.1

4.4. CO_2 Purification Unit (CPU) Integration

4.4.1. Rationale

Achieving both high purity and recovery from VSA is possible if we put fewer constraints on all the operational variables and perform optimization to achieve certain levels of purity and recovery. However, it can lead to unrealistic variables, especially in terms of the low-pressure level in which the vacuum pump works at very low efficiency. On the other hand, it can lead to a very high evacuation period

which makes the footprint so large if we want to maintain continuous feed to our system.

In this work, we have proposed the three scenarios for VSA integrated into a large-scale WtE plant considering the lowest possible footprint. As a result, minimum purity and recovery levels suggested by US-DOE (90% recovery and 95% purity) for a system that can be considered a standard CCUS system that produces CO_2 suitable for either utilization or storage can not be achieved simultaneously.

Due to this fact, we aimed at analyzing the proposed VSA system integrated into a CO_2 purification unit (CPU). The integrated system allows us to reach recovery $\geq$ 90% and purity $\geq$ 95%, simultaneously. Besides, the outlet stream is pressurized to 110 bar which is a standard requirement for transportation, utilization, or storage. The VSA-CPU integrated case is further analyzed to calculate the cost of CO_2 captured.

4.4.2. Process Description

The CO_2 purification unit that is addressed in this work is the Moderate Purity CPU scheme originally developed by Magli et al.[36] The original model is provided by the authors to me and I am allowed to use it in this work. Due to the different characteristics of the gas stream that enters the CPU, some modification is made to the original model.

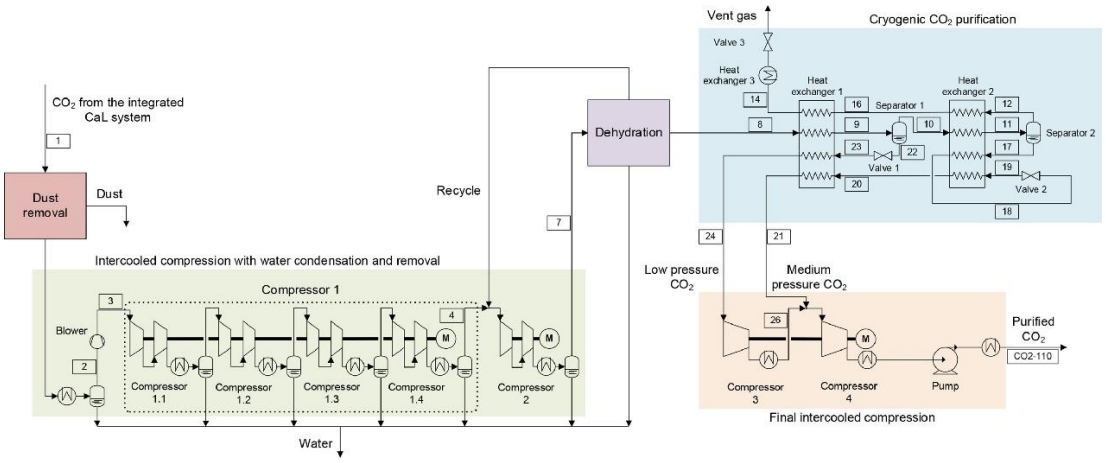

Figure 4.7: Process flow diagram of the Moderate Purity CPU proposed by Magli et al.[36]

As we can see in Figure 4.7, the original model includes a dust removal section and a dehydration unit which is designed based on the feed gas from a calcium looping CO_2 capture system. As in this work, we have simplified the flue gas as a mixture of CO_2 and N_2, these units are not necessary to be applied.

The inlet gas stream enters the CPU from the VSA plant and is compressed in the initial compressor network to the pressure range between $20 - 50\ bar$ which is a design variable given the CPU as an input. Then, the gas stream is purified through cryogenic heat exchanger networks in which the lowest allowable temperature that the hot gas can be reached is a design variable with the lower limit of $-50℃$. Other required variables should be chosen considering the lowest allowable temperature difference of $1℃$ in both heat exchanger networks. Finally, the purified gas is compressed and pumped to $110\ bar$ which is the reference pressure required for CO_2 transportation and storage.

4.4.3. Integrated VSA-CPU System

To make a comparison on the same basis, the following assumptions are taken into account:

1- The target in all the cases is to reach 95% of purity and $110\ bar$ at the outlet of the CPU. This condition is the minimum requirement for transport and storage of CO_2.

2- As in this work, we are targeting a WtE flue gas which around 50% of its CO_2 content has biogenic nature, all the recovery levels $\geq 50\%$ are assumed reasonable. Although we previously targeted the highest possible recovery in all case studies and the lowest recovery is related to Case P with 73.89%. (see Table 4.4).

For Case P, as we have already reached the targeted purity of 95%, the integration of the CPU only plays a role of a compression unit to reach the final pressure of $110\ bar$. This is also valid in the economic assessment that will be performed in the next section.

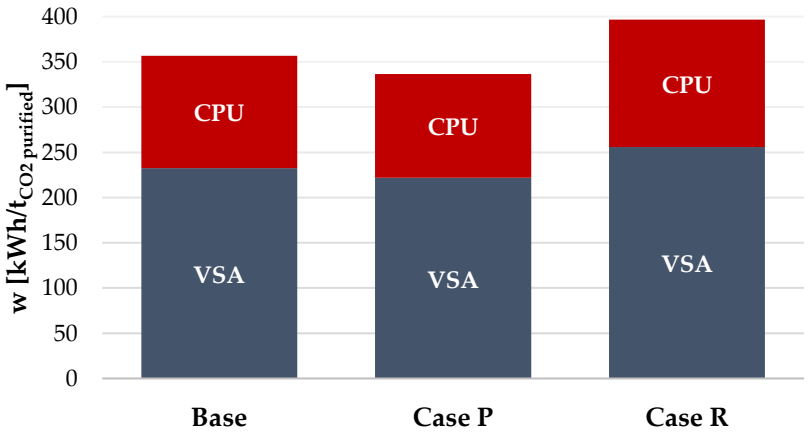

Figure 4.8: Specific work of the integrated VSA-CPU system for the selected cases targeting 95% purity and 110 bar outlet pressure.

It is worth noting that to calculate the specific energy consumption for the integrated system, we should reference all the energy consumption to the final amount of CO_2 exited from the CPU. Hence, instead of the term $\boldsymbol{CO_2\ captured}$ that we have used at the exit of the VSA, we use the term $\boldsymbol{CO_2\ purified}$ to address the total amount of CO_2 which is ultimately captured. Recovery of the CPU is defined based on the relation between these two as below:

$$Recovery_{CPU} = \frac{CO_2\ purified}{CO_2\ captured} \tag{4.5}$$

We can also define the recovery of the integrated VSA-CPU system as:

$$Recovery_{overall} = Recovery_{VSA} \times Recovery_{CPU} \tag{4.6}$$

As a result, the specific energy consumption of the VSA increases by referring it to the final $CO_2\ purified$. In Figure 4.8, we can see the share of both VSA and CPU in the final energy consumption refers to the final $CO_2\ purified$. The base case, results in total energy consumption of $357\frac{kWh}{t_{CO2\ purified}}$. As we aim at reaching higher purity at the expense of lower recovery in Case P, the share of both VSA and CPU decreases and the total energy consumption also decreases to $337\frac{kWh}{t_{CO2\ purified}}$. Case R represents the highest energy consumption as we can reach the highest possible recovery and recovery simultaneously considering the integrated scheme with the total energy consumption value of $397\frac{kWh}{t_{CO2\ purified}}$.

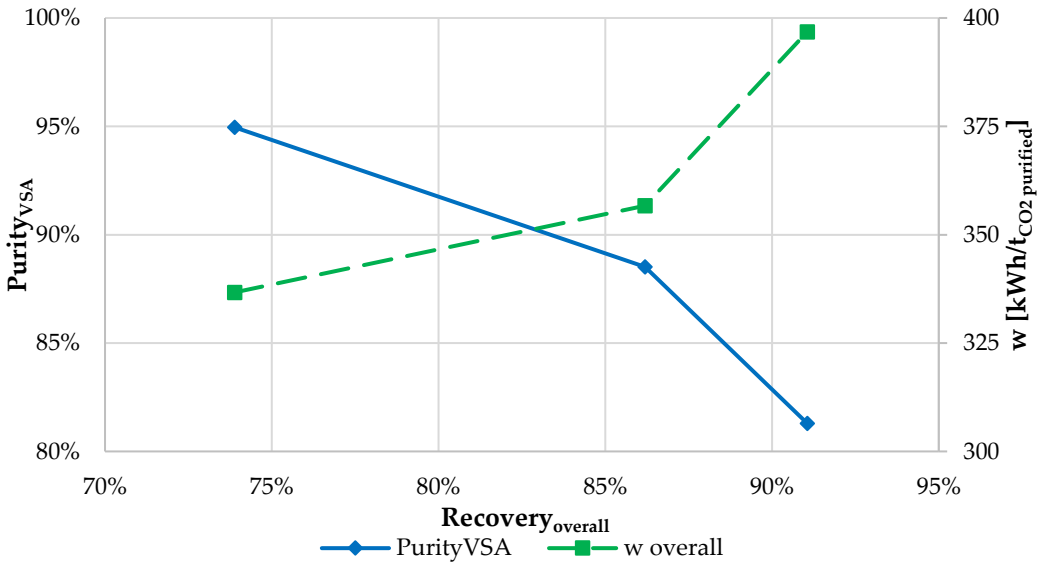

Figure 4.9: Effect of adding CPU to the purity and specific work w.r.t the overall recovery for the selected cases targeting 95% purity and 110 bar outlet pressure.

As represented in Figure 4.9, the high purity case (Case P), ultimately results in the lowest overall recovery of 73.89% which is in this case the same as the recovery of the VSA as the CPU only acts as a compression unit. The recovery of the base case is decreased to 86.19% to make purity increase from 88.51% to 95% in the integrated VSA-CPU scheme. The high recovery case (Case R) has the highest increase in the purity increases from 81.3% to the final level of 95%, at the expense of penalizing the recovery by around 6% and the highest specific energy consumption compared to other cases.

4.5. Economic Assessment

To evaluate the final cost per unit of $CO_2\ purified$, we have used the cost functions reported by Subraveti et al[5] to calculate the cost of each VSA equipment. Regarding the CPU, similar cost functions are reported by Magli et al[36] which are used in this work. In Table 4.5, the relevant economic assumptions are reported.

Table 4.5: Economic assumptions.

Economic lifetime	20 $years$
Capacity factor (CF)	91.30%
Levelized carrying charge (LCC)	10%
Scale factor (SF)	0.66
Discount rate	8%
Intervals of sorbent replacement	$Every$ 5 $years$
Electricity cost[i]	**2022**: 135 €/MWh **2020**: 81 €/MWh
Transportation and storage cost	10 €/t_{CO_2}
Maintenance cost	2.5% $of\ TPC\ per\ year$
Insurance, tax, and administrative cost	2.5% $of\ TPC\ per\ year$

The methodology that used in calculating the total plant cost (TPC) is that after evaluating the equipment cost (EC) based on the cost functions, by proper correction factors that are reported in Table 4.6, we can calculate the TPC as:

$$TPC = EC \times \left(1 + \frac{TDC}{EC}\right) \times \left(1 + \frac{TPC}{TDC}\right) \tag{4.7}$$

Total direct cost (TDC) is taking the process contingencies into account. Besides, further increment of TDC due to the indirect costs, project contingencies, and

[i] Data obtained from ARERA

owner's cost is considered to reach the TPC. The cost of piping is also considered to be included in the project contingencies.

Table 4.6: Correction factor for the calculation of TPC.

Correction factor	VSA	CPU
TDC/EC	15%	32%
TPC/TDC	41%	36%

Wherever the cost functions were not accessible, the scale effect is implemented to calculate the equipment cost from a reference case, using the formula written below:

$$EC = EC_{ref} \times \left(\frac{Actual\ size}{Reference\ size}\right)^{SF} \tag{4.8}$$

This recent scenario is used for flue gas cooling and drying of VSA[5] and the heat exchanger networks of the CPU[37] where the reference parameters are extracted from the cited papers. In Table 4.7, we can see the calculated cost for each process unit as well as the fixed and variable operational costs. All the costs are transformed to the cost of $CO_2\ purified$ for better interpretation.

Table 4.7: Cost breakdown of three case studies.

Cost $\left[\frac{€}{t_{CO2,purified}}\right]$	Base case	Case P	Case R
CAPEX	**30.3**	**34.3**	**29.5**
VSA	24.9	28.7	24.0
FG cooling and drying	5.1	6.0	4.8
Compressor	4.6	5.4	4.3
Columns	5.9	6.9	5.5
Vacuum pumps	2.6	2.4	3.1
Valves	0.5	0.5	0.4
Sorbent	3.1	3.7	2.9
Sorbent replacement	3.2	3.8	3.0
CPU	5.3	5.6	5.5
Fixed OPEX	**15.9**	**18.1**	**15.5**
VSA	13.1	15.1	12.6
CPU	2.8	3.0	2.9
Electricity	**48.2**	**45.5**	**53.6**
VSA	31.4	29.9	34.5
CPU	16.8	15.6	19.0
Transportation and Storage	**10.0**	**10.0**	**10.0**
TOTAL	**104.4**	**107.7**	**108.5**

The calculated valued are in good compliance large-scale VSA design by Subraveti et al.[5] The reported TPC per unit of $CO_2\ purified$ for each unit is the result of splitting the TPC through the plant's lifetime considering the Levelized Carrying Charge (LCC) and capacity factor assumed in Table 4.5. Using equation (4.9), the equivalent cost per unit of $CO_2\ purified$ can be obtained.

$$c_{TPC}\left[\frac{€}{t_{CO2,purified}}\right] = \frac{TPC \times LCC}{P_{overall} \times CF \times 8760} \tag{4.9}$$

As represented in Figure 4.10, the highest VSA cost is related to the Case P where we have the lowest recovery which increases the specific cost per unit tonne of CO_2 extracting from the CPU. Although the lowest share of VSA cost is related to Case R, because of the highest amount of CO_2 is recovered in this case, the vacuum pumps in the VSA and compressors of the CPU handle larger flow rates, meaning higher energy consumption in this case. Due to the high price of electricity that we assumed in this work based on the current electricity crisis that exists in Europe in the year that this study is done (2022), the highest share of prices for both VSA and CPU is related to electricity used.

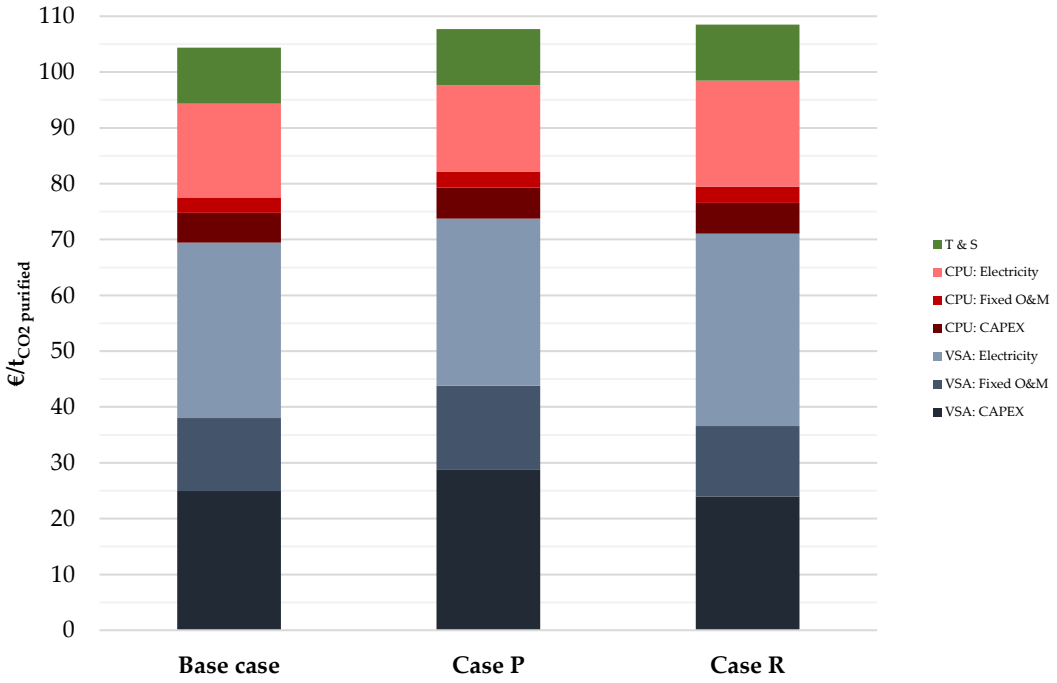

Figure 4.10: Cost breakdown for the three case studies.

Considering Case R, thanks to the high recovery, expressing the VSA capital costs in terms of the cost of $CO_2\ purified$ results in the lowest CAPEX compared to the other two cases. However, the cost of electricity for the VSA is almost equal to the

CAPEX and fixed OPEX of the VSA combined. Although the share of CAPEX and OPEX are almost equal in all three cases, again the high share of electricity used in VSA is most significant for Case R, which ultimately causes it to be the most expensive option. If we consider the electricity price reduce to the levels of 2020, Case R would no more be the most expensive case. We can see the comparison of the total cost of CO_2 *purified* for the electricity price value of 2022 and 2020 in Figure 4.12.

The breakdown of the CAPEX for each case is also represented in Figure 4.11. It is clear that in all cases, the highest share of the CAPEX is related to the final cost of columns. This value is around 6 $\frac{€}{t_{CO2,purified}}$ for Base case and Case R, and reaches 7 $\frac{€}{t_{CO2,purified}}$ for Case P, with lowest recovery level among all the cases. As Case R, with the highest amount of recovery for the same feed rate in all cases, handles the largest volume of gas during blowdown and evacuation steps, the share related to the pumps' cost reaches its maximum for this scenario. Flue gas cooling and drying process contributes to relatively a high share of CAPEX and consequently the total cost of CO_2 *purified*. This confirms the necessity of developing a proper hydrophobic sorbent to handle CO_2 at lower partial pressures. This ultimately decreases the cost of CO_2 *purified* significantly due to eliminating the cooling and drying process.

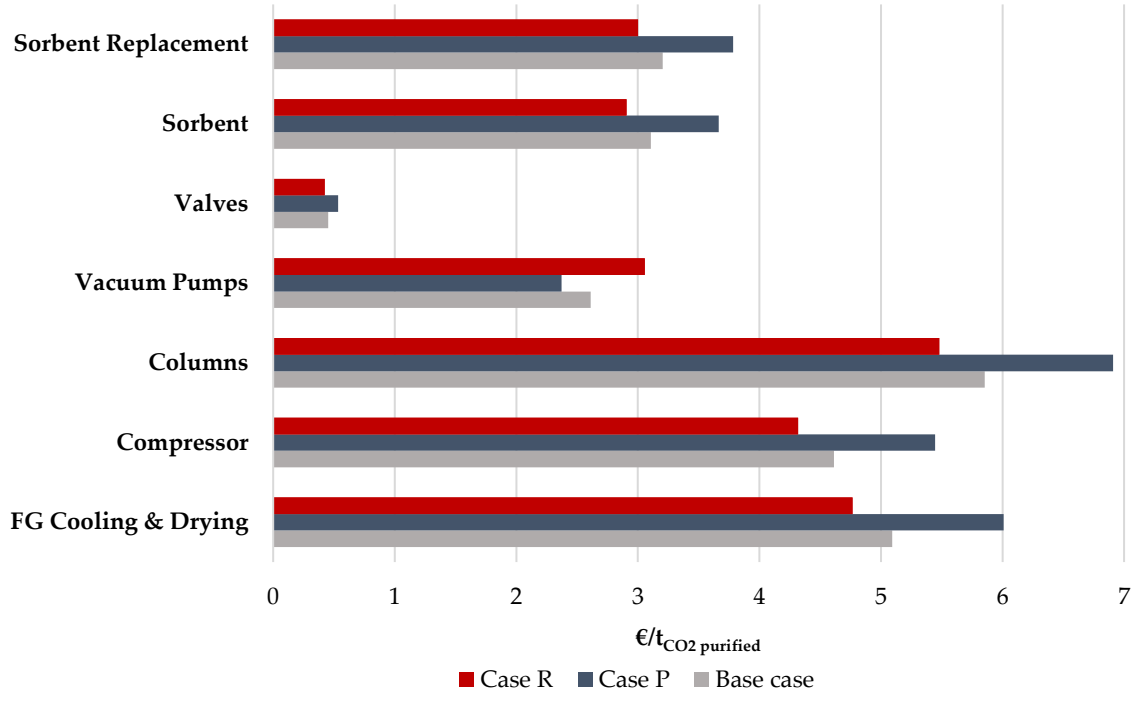

Figure 4.11: Comparison of VSA CAPEX breakdown for three cases.

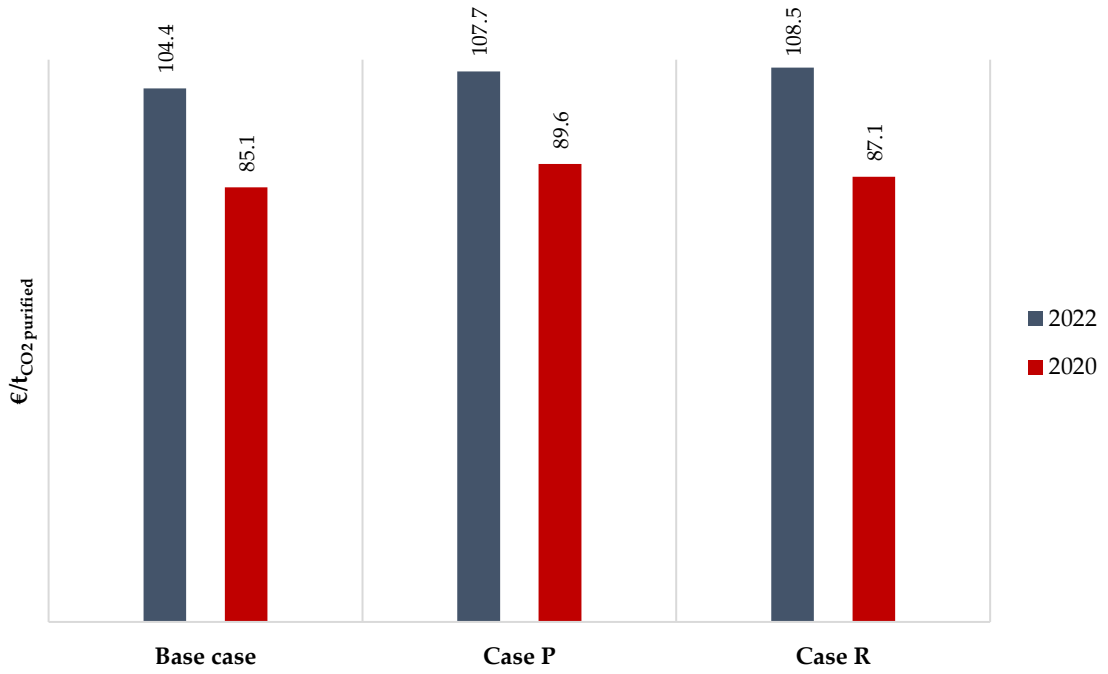

Figure 4.12: Cost of CO_2 purified based on electricity price in 2020 and 2022.

As represented in Figure 4.12, in case the electricity price reduces to its 2020's level, a significant drop in the total cost of $CO_2\ purified$ occurs. As a result, Case P in which the lowest recovery and highest purity are obtained from the VSA system becomes the most expensive scenario. Hence, we can report Case R, as the best case thanks to the overall recovery higher than 90% and a purity level of 95%, with a final cost of 87.1 $\frac{€}{t_{CO2,purified}}$. Although this value is slightly higher than the Base case, as Case R can satisfy the standard requirements of the CO_2 capture systems in terms of purity and recovery, it is reported as the base case scenario.

5 Conclusion

The potential of a 4-step Vacuum-Swing Adsorption (VSA) system for capturing CO_2 in partial pressure range as of post-combustion flue gas is studied in this work. The numerical approach is followed to solve the mass balance equations in a transient state for each of 4 separate process steps for a simplified flue gas consisting of a binary mixture of CO_2 and N_2. After implying proper boundary conditions based on the states of both ends of the column at each step, the component mass balance is solved to calculate the composition of the gas phase at each time step, while the total mass balance is solved to calculate the changes of velocity.

For process modeling of the adsorption system it is important to pay attention to the fact that after assuming the proper strategy of mass transfer between gas and solid (like LDF that is used in this work), we should simultaneously solve the transient mass transfer model coupled with the components mass balance. Then the calculated composition is used to update the velocity field by solving the total mass balance equation. For a more accurate approach that can predict the behavior of the system closer to the real phenomena, these sets of equations should be coupled with instantaneous pressure drop and energy balance to update the pressure and temperature field as well. In this work, we assumed the isothermal assumption which could lead to inaccuracy as it does not consider the expansion of the gas phase during the adsorption where the heat is released or similarly, the effect of the endothermic desorption process occurs in the regenerating steps.

To have a more accurate picture of how the process works at a large scale, the implementation of the VSA in a WtE is studied. Due to the high number of operational variables that affect the performance of the VSA, we limited our scope to three main variables namely the low and intermediate pressure levels, and the adsorption time by performing a sort of parametric analysis. Although cycle optimization is an inseparable part of VSA system design and evaluation, by this means, we directed our focus to evaluate process performances for the lowest possible footprint which is the main obstacle that resists speeding up the development of VSA on a large scale.

Three scenarios are defined and discussed in terms of main performance indicators and cost of $CO_2\,purified$, on the same basis of capturing CO_2 ultimately at 95%

purity and 110 bar. The results showed lower energy consumption compared to the benchmark MEA technology which is consistent with the results reported by scientific literature in this field. However, some important levels of uncertainties are identified that have crucial importance before deciding to further elevate the TRL of such projects.

The first and most important one is the low vacuum pump efficiency at the low-pressure levels that should be provided in VSA schemes. In this work, we used the efficiency value of 72% which is a typical value for vacuum pump efficiency to make us able to compare our results with relevant literature. But this drop in efficiency should be further analyzed and tested as it can ultimately result in an even higher energy penalty compared to the benchmark MEA process on the same energy bases (i.e. taking into account the transformation of thermal energy into electrical energy).

Developing sorbent material to handle the water content of the real flue gas is another subject of research and development direction in this field. Most of the literature considers the simplified flue gas in the process modelling that could be one of the main sources of inaccuracy to predict the real behavior of the process itself. Additional simplifying assumptions such as isothermal adsorption and negligible pressure drop alongside the column in the modelling procedure should be kept in mind before relying on the results previously built based on such simplifying assumptions.

The potential development of this work can be defined based on the mentioned challenges. Coupling the mass balance equation with pressure drop and energy balance equations, while considering a more realistic flue gas composition is the main target that will be followed. Furthermore, implementing more promising sorbent data (such as MOFs) in the model can be targeted to compare different sorbent's performance in the post-combustion CO_2 capture application. Due to the important issue about the vacuum pump efficiency as previously discussed, the performance curve of several commercial vacuum pumps can be taken into account instead of a simplified assumption of efficiency, hence we will be able to enhance our understanding of this source of inaccuracy.

Bibliography

(1) Raganati, F.; Miccio, F.; Ammendola, P. Adsorption of Carbon Dioxide for Post-Combustion Capture: A Review. *Energy Fuels* **2021**, *35* (16), 12845–12868. https://doi.org/10.1021/acs.energyfuels.1c01618.

(2) Jiang, N.; Shen, Y.; Liu, B.; Zhang, D.; Tang, Z.; Li, G.; Fu, B. CO2 Capture from Dry Flue Gas by Means of VPSA, TSA and TVSA. *J. CO2 Util.* **2020**, *35*, 153–168. https://doi.org/10.1016/j.jcou.2019.09.012.

(3) Riboldi, L.; Bolland, O. Evaluating Pressure Swing Adsorption as a CO2 Separation Technique in Coal-Fired Power Plants. *Int. J. Greenh. Gas Control* **2015**, *39*, 1–16. https://doi.org/10.1016/j.ijggc.2015.02.001.

(4) Haghpanah, R.; Majumder, A.; Nilam, R.; Rajendran, A.; Farooq, S.; Karimi, I. A.; Amanullah, M. Multiobjective Optimization of a Four-Step Adsorption Process for Postcombustion CO 2 Capture Via Finite Volume Simulation. *Ind. Eng. Chem. Res.* **2013**, *52* (11), 4249–4265. https://doi.org/10.1021/ie302658y.

(5) Subraveti, S. G.; Roussanaly, S.; Anantharaman, R.; Riboldi, L.; Rajendran, A. Techno-Economic Assessment of Optimised Vacuum Swing Adsorption for Post-Combustion CO2 Capture from Steam-Methane Reformer Flue Gas. *Sep. Purif. Technol.* **2021**, *256*, 117832. https://doi.org/10.1016/j.seppur.2020.117832.

(6) Plaza, M. G.; García, S.; Rubiera, F.; Pis, J. J.; Pevida, C. Post-Combustion CO2 Capture with a Commercial Activated Carbon: Comparison of Different Regeneration Strategies. *Chem. Eng. J.* **2010**, *163* (1–2), 41–47. https://doi.org/10.1016/j.cej.2010.07.030.

(7) Hefti, M.; Marx, D.; Joss, L.; Mazzotti, M. Adsorption Equilibrium of Binary Mixtures of Carbon Dioxide and Nitrogen on Zeolites ZSM-5 and 13X. *Microporous Mesoporous Mater.* **2015**, *215*, 215–228. https://doi.org/10.1016/j.micromeso.2015.05.044.

(8) Samanta, A.; Zhao, A.; Shimizu, G. K. H.; Sarkar, P.; Gupta, R. Post-Combustion CO 2 Capture Using Solid Sorbents: A Review. *Ind. Eng. Chem. Res.* **2012**, *51* (4), 1438–1463. https://doi.org/10.1021/ie200686q.

(9) Maring, B. J.; Webley, P. A. A New Simplified Pressure/Vacuum Swing Adsorption Model for Rapid Adsorbent Screening for CO2 Capture Applications. *Int. J. Greenh. Gas Control* **2013**, *15*, 16–31. https://doi.org/10.1016/j.ijggc.2013.01.009.

(10) Dhoke, C.; Zaabout, A.; Cloete, S.; Amini, S. Review on Reactor Configurations for Adsorption-Based CO 2 Capture. *Ind. Eng. Chem. Res.* **2021**, *60* (10), 3779–3798. https://doi.org/10.1021/acs.iecr.0c04547.

(11) Silva, E.; Llewellyn, P.; Kumar, P.; Webley, P. A. Technology Options for CO 2 Adsorption. *SSRN Electron. J.* **2021**. https://doi.org/10.2139/ssrn.3821077.

(12) Joss, L.; Gazzani, M.; Mazzotti, M. Rational Design of Temperature Swing Adsorption Cycles for Post-Combustion CO 2 Capture. *Chem. Eng. Sci.* **2017**, *158*, 381–394. https://doi.org/10.1016/j.ces.2016.10.013.

(13) van Paasen, S.; Infantino, M.; Yao, J.; Leenders, S. H. A. M.; van de Graaf, J. M.; Klingler, A.; Zerobin, F.; Pröll, T.; Schöny, G.; Fuchs, J.; Hofbauer, H. Development of the Solid Sorbent Technology for Post Combustion CO2 Capture towards Commercial Prototype. *Int. J. Greenh. Gas Control* **2021**, *109*, 103368. https://doi.org/10.1016/j.ijggc.2021.103368.

(14) Dhoke, C.; Zaabout, A.; Cloete, S.; Seo, H.; Park, Y.; Blom, R.; Amini, S. The Swing Adsorption Reactor Cluster (SARC) for Post Combustion CO2 Capture: Experimental Proof-of-Principle. *Chem. Eng. J.* **2019**, *377*, 120145. https://doi.org/10.1016/j.cej.2018.10.082.

(15) Dhoke, C.; Zaabout, A.; Cloete, S.; Seo, H.; Park, Y.; Demoulin, L.; Amini, S. Demonstration of the Novel Swing Adsorption Reactor Cluster Concept in a Multistage Fluidized Bed with Heat-Transfer Surfaces for Postcombustion CO 2 Capture. *Ind. Eng. Chem. Res.* **2020**, *59* (51), 22281–22291. https://doi.org/10.1021/acs.iecr.0c05951.

(16) Skarstrom, C. W. Method and Apparatus for Fractionating Gaseous Mixtures by Adsorption, 1960.

(17) Quaranta, I. C. C.; Pinheiro, L. S.; Gonçalves, D. V.; Peixoto, H. R.; Lucena, S. M. P. Multiscale Design of a Pressure Swing Adsorption Process for Natural Gas Purification. *Adsorption* **2021**, *27* (7), 1055–1066. https://doi.org/10.1007/s10450-021-00330-y.

(18) Liu, Z.; Grande, C. A.; Li, P.; Yu, J.; Rodrigues, A. E. Multi-Bed Vacuum Pressure Swing Adsorption for Carbon Dioxide Capture from Flue Gas. *Sep. Purif. Technol.* **2011**, *81* (3), 307–317. https://doi.org/10.1016/j.seppur.2011.07.037.

(19) Wang, L.; Yang, Y.; Shen, W.; Kong, X.; Li, P.; Yu, J.; Rodrigues, A. E. CO 2 Capture from Flue Gas in an Existing Coal-Fired Power Plant by Two Successive Pilot-Scale VPSA Units. *Ind. Eng. Chem. Res.* **2013**, *52* (23), 7947–7955. https://doi.org/10.1021/ie4009716.

(20) Wawrzyńczak, D.; Majchrzak-Kucęba, I.; Srokosz, K.; Kozak, M.; Nowak, W.; Zdeb, J.; Smółka, W.; Zajchowski, A. The Pilot Dual-Reflux Vacuum Pressure Swing Adsorption Unit for CO2 Capture from Flue Gas. *Sep. Purif. Technol.* **2019**, *209*, 560–570. https://doi.org/10.1016/j.seppur.2018.07.079.

(21) Zhang, J.; Webley, P. A. Cycle Development and Design for CO 2 Capture from Flue Gas by Vacuum Swing Adsorption. *Environ. Sci. Technol.* **2008**, *42* (2), 563–569. https://doi.org/10.1021/es0706854.

(22) Nikolaidis, G. N.; Kikkinides, E. S.; Georgiadis, M. C. Model-Based Approach for the Evaluation of Materials and Processes for Post-Combustion Carbon Dioxide Capture from Flue Gas by PSA/VSA Processes. *Ind. Eng. Chem. Res.* **2016**, *55* (3), 635–646. https://doi.org/10.1021/acs.iecr.5b02845.

(23) Haghpanah, R.; Nilam, R.; Rajendran, A.; Farooq, S.; Karimi, I. A. Cycle Synthesis and Optimization of a VSA Process for Postcombustion CO 2 Capture. *AIChE J.* **2013**, *59* (12), 4735–4748. https://doi.org/10.1002/aic.14192.

(24) Krishnamurthy, S.; Rao, V. R.; Guntuka, S.; Sharratt, P.; Haghpanah, R.; Rajendran, A.; Amanullah, M.; Karimi, I. A.; Farooq, S. CO 2 Capture from Dry Flue Gas by Vacuum Swing Adsorption: A Pilot Plant Study. *AIChE J.* **2014**, *60* (5), 1830–1842. https://doi.org/10.1002/aic.14435.

(25) Maruyama, R. T.; Pai, K. N.; Subraveti, S. G.; Rajendran, A. Improving the Performance of Vacuum Swing Adsorption Based CO2 Capture under Reduced Recovery Requirements. *Int. J. Greenh. Gas Control* **2020**, *93*, 102902. https://doi.org/10.1016/j.ijggc.2019.102902.

(26) Subraveti, S. G.; Roussanaly, S.; Anantharaman, R.; Riboldi, L.; Rajendran, A. How Much Can Novel Solid Sorbents Reduce the Cost of Post-Combustion CO 2 Capture? A Techno-Economic Investigation on the Cost Limits of Pressure–Vacuum Swing Adsorption. *Appl. Energy* **2022**, *306*, 117955. https://doi.org/10.1016/j.apenergy.2021.117955.

(27) Chue, K. T.; Kim, J. N.; Yoo, Y. J.; Cho, S. H.; Yang, R. T. Comparison of Activated Carbon and Zeolite 13X for CO2 Recovery from Flue Gas by Pressure Swing Adsorption. *Ind. Eng. Chem. Res.* **1995**, *34* (2), 591–598. https://doi.org/10.1021/ie00041a020.

(28) Ko, D.; Siriwardane, R.; Biegler, L. T. Optimization of Pressure Swing Adsorption and Fractionated Vacuum Pressure Swing Adsorption Processes for CO 2 Capture. *Ind. Eng. Chem. Res.* **2005**, *44* (21), 8084–8094. https://doi.org/10.1021/ie050012z.

(29) Dantas, T. L. P.; Luna, F. M. T.; Silva Jr, I. J.; Torres, A. E. B.; de Azevedo, D. C. S.; Rodrigues, A. E.; Moreira, R. F. P. M. Modeling of the Fixed - Bed Adsorption of Carbon Dioxide and a Carbon Dioxide - Nitrogen Mixture on Zeolite 13X. *Braz. J. Chem. Eng.* **2011**, *28* (3), 533–544. https://doi.org/10.1590/S0104-66322011000300018.

(30) IEAGHG, "CCS on Waste to Energy", 2020-06, December 2020.

(31) Fagerlund, J.; Zevenhoven, R.; Thomassen, J.; Tednes, M.; Abdollahi, F.; Thomas, L.; Nielsen, C. J.; Mikoviny, T.; Wisthaler, A.; Zhu, L.; Biliyok, C.; Zhurkin, A. Performance of an Amine-Based CO2 Capture Pilot Plant at the Fortum Oslo Varme Waste to Energy Plant in Oslo, Norway. *Int. J. Greenh. Gas Control* **2021**, *106*, 103242. https://doi.org/10.1016/j.ijggc.2020.103242.

(32) Huttenhuis, P.; Roeloffzen, A.; Versteeg, G. CO2 Capture and Re-Use at a Waste Incinerator. *Energy Procedia* **2016**, *86*, 47–55. https://doi.org/10.1016/j.egypro.2016.01.006.

(33) Bisinella, V.; Nedenskov, J.; Riber, C.; Hulgaard, T.; Christensen, T. H. Environmental Assessment of Amending the Amager Bakke Incineration Plant in Copenhagen with Carbon Capture and Storage. *Waste Manag. Res. J. Sustain. Circ. Econ.* **2022**, *40* (1), 79–95. https://doi.org/10.1177/0734242X211048125.

(34) Djurberg R , Practical Implementation of Bio CCS in Uppsala; A Techno Economic Assessment.

(35) Danaci, D.; Webley, P. A.; Petit, C. Guidelines for Techno-Economic Analysis of Adsorption Processes. *Front. Chem. Eng.* **2021**, *2*, 602430. https://doi.org/10.3389/fceng.2020.602430.

(36) Magli, F.; Spinelli, M.; Fantini, M.; Romano, M. C.; Gatti, M. Techno-Economic Optimization and off-Design Analysis of CO2 Purification Units for Cement Plants with Oxyfuel-Based CO2 Capture. *Int. J. Greenh. Gas Control* **2022**, *115*, 103591. https://doi.org/10.1016/j.ijggc.2022.103591.

(37) Gardarsdottir, S.; De Lena, E.; Romano, M.; Roussanaly, S.; Voldsund, M.; Pérez-Calvo, J.-F.; Berstad, D.; Fu, C.; Anantharaman, R.; Sutter, D.; Gazzani, M.; Mazzotti, M.; Cinti, G. Comparison of Technologies for CO2 Capture from Cement Production—Part 2: Cost Analysis. *Energies* **2019**, *12* (3), 542. https://doi.org/10.3390/en12030542.

List of Figures

List of Tables

List of symbols

Variable	Description	SI unit
A	Column cross-sectional area	m^2
C	Gas phase concentration	$\frac{mol}{m^3}$
d_p	Adsorbent particle diameter	m
D	Column diameter	m
D_e	Effective gas diffusivity	$\frac{m^2}{s}$
D_L	Axial dispersion coefficient	$\frac{m^2}{s}$
D_m	Molecular diffusivity	$\frac{m^2}{s}$
D_p	Effective macropore diffusivity	$\frac{m^2}{s}$
ε_b	Porosity of bed: the volume fraction of void space inside bed w.r.t the bed volume	$-$
ε_p	Porosity of adsorbent particle	$-$
η	Efficiency	$-$
γ	Adiabatic constant	$-$
K	Slope of the equilibrium isotherm with consistent units	$-$
L	Length	m
μ	Fluid viscosity	$\frac{kg}{m.s}$
N	Moles	mol
p	Pressure	Pa

P	Power	W
q	Solid phase concentration	$\frac{mol}{kg}$
q^*	Saturation capacity of gas in the solid	$\frac{mol}{kg}$
ρ	Fluid density	$\frac{kg}{m^3}$
ρ_s	Adsorbent density	$\frac{kg}{m^3}$
r_p	Adsorbent particle radius	m
R	Universal gas constant	$\frac{J}{mol.K}$
τ	Tortuosity	$-$
t	Time	s
T	Temperature	K
u	Interstitial gas velocity	$\frac{m}{s}$
v	Superficial gas velocity	$\frac{m}{s}$
V	Volume	m^3
W	Work	J
y	Gas phase composition	$-$
z	Axial direction of the column	m

Acknowledgments

My special thanks to Politecnico di Milano and Italy, for this opportunity in the past 3 years to develop myself not only scientifically but also as a person.

I would like to thank Professor Manuele Gatti for his guidance in developing a fruitful path for this thesis work and for his mutual understanding of the challenges during this journey.

I express my deepest gratitude to my family and my dear Zahra for all their support and encouragement during this chapter of my life.

Piacenza – October 2022

Nima